SHIP2 negatively regulates the insulin-induced translocation and phosphorylation of Akt2 at the PM mediated via both the IRS-1 and IRS-2 pathway.

EXPERIMENTAL PROCEDURES

Materials—Human crystal insulin was provided by Novo Nordisk Pharmaceutical Co., (Copenhagen, Denmark). The two polyclonal anti-SHIP2 antibodies were described previously (5). The anti-SHIP2 antibodies raised against the C terminus and N terminus were used for the immunoprecipitation and immunoblotting, respectively. A monoclonal anti-phosphotyrosine antibody (PY20) was purchased from Transduction Laboratories (Lexington, KY). A polyclonal anti-Thr^{308} phospho-specific Akt antibody and a polyclonal anti-Ser^{473} phospho-specific Akt antibody were obtained from New England Biolabs, Inc. (Beverly, MA). A polyclonal anti-Akt antibody and a polyclonal anti-Akt1-specific antibody were from Santa Cruz Biotechnology (Santa Cruz, CA). A polyclonal anti-Akt2-specific antibody was from Calbiochem. Enhanced chemiluminescence reagents were from Amersham Biosciences. Dulbecco's modified Eagle's medium (DMEM), minimum essential medium vitamin mixtures, and minimum essential medium amino acid solutions were from Invitrogen. All other reagents were of analytical grade and purchased from Sigma or Wako Pure Chemical Industries, Ltd. (Osaka, Japan).

Construction of Adenoviral Vectors—cDNAs encoding rat WT-SHIP2 and ΔIP-SHIP2 were subcloned into the vector pAxCAwt and transferred to recombinant adenovirus by homologous recombination utilizing an adenovirus expression vector kit (Takara Biomedicals, Tokyo, Japan) as described previously (7). The adenoviral vector encoding the constitutively active form of bovine p110 with a Src myristration signal sequence at the N terminus (myr-p110) was reported previously (21).

Cell Culture and Infection with Adenovirus—3T3-L1 fibroblasts were grown and passaged in DMEM supplemented with 10% newborn calf serum. Cells at 2 to 3 days post-confluence were used for differentiation. The differentiation medium contained 10% fetal calf serum (FCS), 250 nM dexamethasone, 0.5 mM isobutyl methylxanthine, and 500 nM insulin. After 3 days, the differentiation medium was replaced with post-differentiation medium containing 10% FCS and 500 nM insulin. After 3 more days, the post-differentiation medium was replaced with DMEM supplemented with 10% FCS (7). Preparation of IRS-1(−/−) and IRS-2(−/−) embryonic fibroblasts from IRS-1- and IRS-2-deficent mice was described previously (22). Embryonic fibroblasts were cultured with α-minimum essential medium supplemented with 10% FCS. WT-SHIP2, ΔIP-SHIP2, and myr-p110 were transiently expressed in differentiated 3T3-L1 adipocytes and embryonic fibroblasts by means of adenovirus-mediated gene transfer. A multiplicity of infection (m.o.i.) of 10–40 pfu/cell was used to infect 3T3-L1 adipocytes and embryonic fibroblasts in DMEM containing 2% FCS, with the virus being left on the cells for 16 h prior to removal. Subsequent experiments were conducted 24 to 48 h after initial addition of the virus. The efficiency of the adenovirus-mediated gene transfer of WT-SHIP2, ΔIP-SHIP2, and myr-p110 was ~95%.

Subcellular Fractionation—3T3-L1 adipocytes were washed twice with phosphate-buffered saline and once with HES buffer (255 mM sucrose, 20 mM HEPES, 1 mM EDTA, 1 mM phenylmethylsulfonyl fluoride, 1 mM Na_3VO_4, 2 μg/ml aprotinin, and 50 ng/ml okadaic acid, pH 7.4) and immediately homogenized by 20 strokes with a motor-driven homogenizer in HES buffer at 4 °C. The homogenates (two 10-cm-diameter dishes per condition) were subjected to subcellular fractionation as described previously to isolate PM, high density microsomes, low density microsomes (LDM), and cytosol (23, 24). In brief, the homogenates were centrifuged at 19,000 × *g* for 20 min. The resulting supernatant was centrifuged at 41,000 × *g* for 20 min, yielding a pellet of high density microsomes. The supernatant from this spin was centrifuged at 250,000 × *g* for 90 min, yielding a pellet of LDM. Remaining supernatant was concentrated by Centricon-30 (Amicon Inc., Beverly, Mass.) and used as cytosol. The pellet obtained from the initial spin was resuspended in HES buffer, layered onto a 1.12 M sucrose cushion, and centrifuged at 100,000 × *g* in a swing rotor for 60 min. A white fluffy band at the interface was collected and resuspended in HES buffer and centrifuged at 40,000 × *g* for 20 min, yielding a pellet of PM. All fractions were adjusted to a final protein concentration of 1 to 3 mg/ml, which was measured by the Bradford method, and stored at −80 °C until use.

Immunoprecipitation and Western Blotting—3T3-L1 adipocytes and embryonic fibroblasts grown in 6-well multiplates were serum-starved for 16 h in DMEM. The cells were treated with 17 nM insulin at 37 °C for various periods. They were then lysed in a buffer containing 20 mM Tris, 150 mM NaCl, 1 mM EDTA, 1 mM EGTA, 2.5 mM sodium deoxycholate, 1 mM β-glycerophosphate, 1% Triton X-100, 1 mM phenylmethylsulfonyl fluoride, 1 mM Na_3VO_4, 50 mM sodium fluoride, 10 μg/ml aprotinin, and 10 μM leupeptin, pH 7.4, for 15 min at 4 °C. Lysates obtained from the same number of cells were centrifuged to remove insoluble materials. The supernatants (100 μg of protein) were immunoprecipitated with antibodies for 2 h at 4 °C. The precipitates or whole cell lysates were then separated by 7.5% SDS-PAGE and transferred onto polyvinylidene difluoride membranes using a Bio-Rad Transblot apparatus. The membranes were blocked in a buffer containing 50 mM Tris, 150 mM NaCl, 0.1% Tween 20, and 2.5% bovine serum albumin or 5% non-fat milk, pH 7.5, for 2 h at 20 °C. The membranes were then probed with antibodies for 2 h at 20 °C or for 16 h at 4 °C. After the membranes were washed in a buffer containing 50 mM Tris, 150 mM NaCl, and 0.1% Tween 20, pH 7.5, blots were incubated with a horseradish peroxidase-linked secondary antibody and subjected to enhanced chemiluminescence detection using ECL reagent according to the manufacturer's instructions (Amersham Biosciences) (5, 7).

Statistical Analysis—The data are represented as means ± S.E. *p* values were determined using a Student's *t* test, and $p < 0.05$ was considered statistically significant.

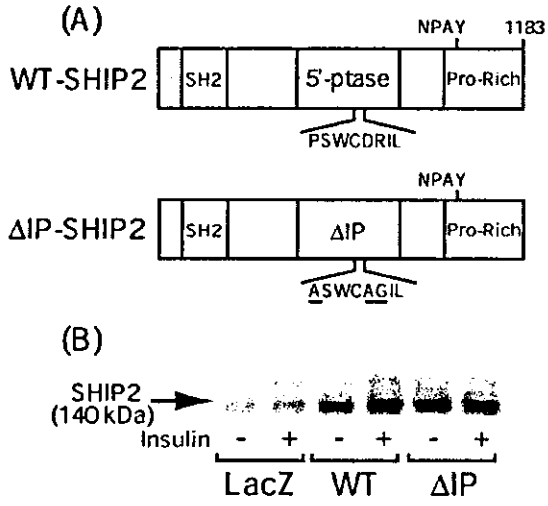

FIG. 1. **Structures of SHIP2 constructs and expression in 3T3-L1 adipocytes.** *A*, structures of wild-type SHIP2 and 5′-phosphatase-defective SHIP2 containing Pro^{687} to Ala, Asp^{691} to Ala, and Arg^{692} to Gly changes are shown. The three domains of SHIP2 are an SH2 domain, a 5′-phosphatase (*5′-ptase*) domain, and a C-terminal proline-rich domain containing a tyrosine phosphorylation site (*NPAY*). *B*, 3T3-L1 adipocytes were transfected with LacZ, WT-SHIP2, or ΔIP-SHIP2 at an m.o.i. of 40 pfu/cell. Following the infection, the cells were stimulated with 17 nM insulin for 5 min. The cells were lysed and subjected to immunoblot analysis with anti-SHIP2 antibody. Results are representative of three separate experiments.

RESULTS

Structures of SHIP2 Constructs and the Expression in 3T3-L1 Adipocytes—SHIP2 is a 140-kDa protein composed of an SH2 domain at the N terminus, a central 5′-phosphatase catalytic domain, and a proline-rich region including the phosphotyrosine binding domain binding consensus at the C terminus. Three amino acids, located within the catalytic domain of SHIP2, that are highly conserved among known 5′-phosphatases were mutated to generate ΔIP-SHIP2 (7) (Fig. 1*A*). WT-SHIP2 and ΔIP-SHIP2 were transiently expressed in 3T3-L1 adipocytes by adenovirus-mediated gene transfer. Endogenous SHIP2 was seen in control 3T3-L1 adipocytes transfected with LacZ alone. On transfection with either WT-SHIP2 or ΔIP-SHIP2 at an m.o.i. of 40 pfu/cell, we observed similar levels of expression of WT-SHIP2 and ΔIP-SHIP2, which were 5-fold greater than the levels of endogenous SHIP2. Insulin treatment did not affect the expression of WT-SHIP2 and ΔIP-SHIP2 (Fig. 1*B*).

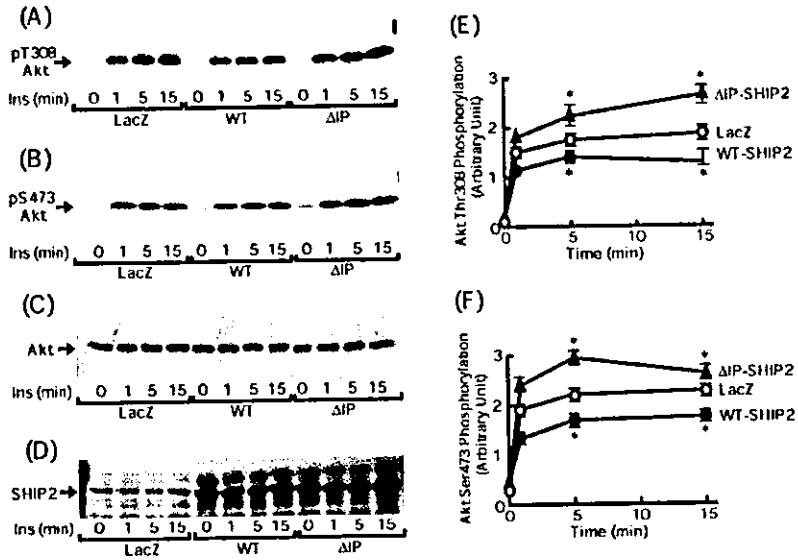

FIG. 2. **Effect of SHIP2 overexpression on insulin-induced phosphorylation of Akt in whole cell lysates.** 3T3-L1 adipocytes were transfected with LacZ (○-○), WT-SHIP2 (●-●), or ΔIP-SHIP2 (▲-▲) at an m.o.i. of 40 pfu/cell. The cells were serum-starved for 16 h and treated with 17 nM insulin for the periods indicated. The cell lysates were separated by 7.5% SDS-PAGE and immunoblotted with anti-Thr^{308}-phospho-specific (*A*) or anti-Ser^{473}-phosphospecific (*B*) Akt antibody. *C*, the cell lysates were immunoblotted with anti-Akt antibody. *D*, the cell lysates were immunoblotted with anti-SHIP2 antibody. The amount of Akt phosphorylated at Thr^{308} (*E*) and Ser^{473} (*F*) corrected for the amount loaded was quantitated by densitometry. Results are means ± S.E. of four separate experiments. *, $p < 0.05$ *versus* the phosphorylation of Akt at respective concentrations of insulin in LacZ-transfected control cells using the Student's *t* test.

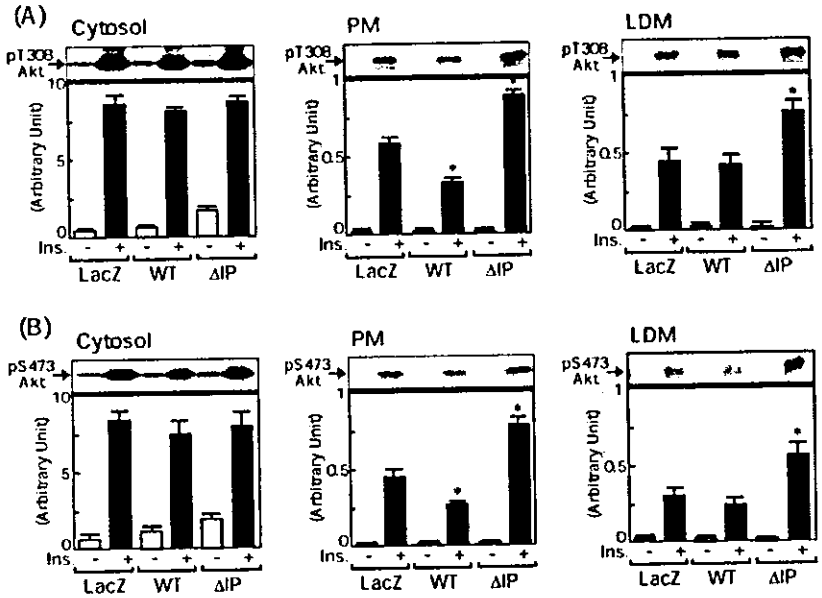

FIG. 3. **Effect of SHIP2 expression on insulin-induced phosphorylation of Akt in subcellular fractions.** 3T3-L1 adipocytes were transfected with LacZ, WT-SHIP2, or ΔIP-SHIP2 at an m.o.i. of 40 pfu/cell. The cells were serum-starved for 16 h and then treated with 17 nM insulin for 5 min. The cells were homogenized and subjected to subcellular fractionation to yield the cytosol, LDM, and PM fractions. Samples in each fraction were separated by SDS-PAGE and immunoblotted with anti-Thr^{308}-phospho-specific (*A*) or anti-Ser^{473}-phosphospecific (*B*) Akt antibody. The amount of Akt phosphorylated at Thr^{308} and Ser^{473} corrected for the amount loaded was quantitated by densitometry. Results are means ± S.E. of four separate experiments. *, $p < 0.05$ *versus* the phosphorylation of Akt after insulin stimulation in LacZ-transfected control cells using the Student's *t* test.

Effect of SHIP2 Expression on Insulin-induced Phosphorylation of Akt in Whole Cell Lysates—Akt is a downstream target of PI3-kinase important for mediation of the metabolic actions of insulin (1–4). Because Akt is primarily activated as a result of its phosphorylation at the Thr^{308} (Akt2 at Thr^{309}) and Ser^{473} (Akt2 at Ser^{474}) residues (13, 16–20, 25), we examined the effect of SHIP2 expression on the insulin-induced phosphorylation of Akt in 3T3-L1 adipocytes. Treatment with insulin induced phosphorylation of Akt at Thr^{308} and Ser^{473} in a time-dependent manner in LacZ-transfected control 3T3-L1 adipocytes. Transfection of WT-SHIP2 decreased insulin-induced phosphorylation of Akt at both Thr^{308} and Ser^{473}. In contrast, insulin-induced phosphorylation of Akt at Thr^{308} and Ser^{473} was increased by transfection with ΔIP-SHIP2 (Fig. 2, *A* and *B*). These results are summarized in Fig. 2, *E* and *F*. Following 15 min of insulin treatment, the phosphorylation of Akt at Thr^{308} was significantly decreased 30.1 ± 4.9% by the expression of WT-SHIP2 and increased 34.6 ± 5.7% by the expression of ΔIP-SHIP2. Similarly, the phosphorylation of Akt at Ser^{473} was decreased 27.9 ± 3.4% by the expression of WT-SHIP2 and increased 31.8 ± 4.4% by the expression of ΔIP-SHIP2 following 5 min of insulin stimulation compared with that in control 3T3-L1 adipocytes transfected with LacZ. To assure equal amounts of protein were loaded among the samples, the cell lysates were immunoblotted with anti-Akt antibody (Fig. 2*C*). Similar expression levels of WT-SHIP2 and ΔIP-SHIP2 were detected on the immunoblotting of the cell lysates with anti-SHIP2 antibody (Fig. 2*D*).

Effect of SHIP2 Expression on Insulin-induced Phosphorylation of Akt at Subcellular Locations—Because it is known that Akt is localized in the cytosol, PM, and LDM fractions (10), we next examined the effect of SHIP2 expression on the insulin-induced phosphorylation of Akt at subcellular locations (Fig. 3). Insulin induced the phosphorylation of Akt at Thr^{308} and Ser^{473} in the cytosol, PM, and LDM fractions. Although a large amount of Akt resides in the cytosol, the insulin-induced phosphorylation of Akt at Thr^{308} and Ser^{473} in the cytosol was not significantly affected by the expression

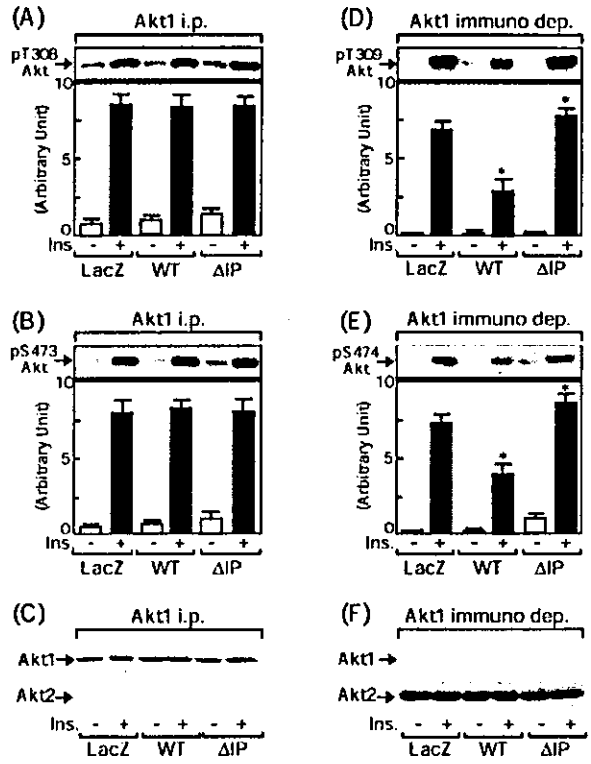

FIG. 4. **Effect of SHIP2 expression on insulin-induced phosphorylation of Akt1 and Akt2 isoforms.** 3T3-L1 adipocytes were transfected with LacZ, WT-SHIP2, or ΔIP-SHIP2 at an m.o.i. of 40 pfu/cell. The cells were serum-starved for 16 h and then treated with 17 nM insulin for 5 min. The cell lysates were immunoprecipitated with anti-Akt1 antibody. The precipitates (*A-C*) and the supernatants (*D-F*) were separated by SDS-PAGE and immunoblotted with anti-Thr^{308}-phospho-specific Akt antibody (*A* and *D*), anti-Ser^{473}-phosphospecific Akt antibody (*B* and *E*), or anti-Akt1 and anti-Akt2 antibody (*C* and *F*). The amount of Akt1 and Akt2 phosphorylated at $Thr^{308/309}$ and $Ser^{473/474}$ corrected for the amount loaded was quantitated by densitometry. Results are means ± S.E. of four separate experiments. *, $p < 0.05$ *versus* the phosphorylation of Akt after insulin stimulation in LacZ-transfected control cells using the Student's *t* test.

of either WT-SHIP2 or ΔIP-SHIP2. In contrast, the phosphorylation of Akt in the PM and LDM was affected by the expression of SHIP2. Notably, the insulin-induced phosphorylation of Akt at both Thr^{308} and Ser^{473} in the PM fraction was markedly decreased by the expression of WT-SHIP2, whereas it was increased by the expression of ΔIP-SHIP2. Densitometric analysis revealed that insulin-induced phosphorylation of Akt at Thr^{308} and Ser^{473} was decreased by 47.3 ± 1.2% and 45.7 ± 3.1%, respectively, in WT-SHIP2-expressing cells, whereas it was enhanced by 44.3 ± 5.6% and 45.3 ± 6.6% in ΔIP-SHIP2-expressing cells.

Effect of SHIP2 Expression on Insulin-induced Phosphorylation of Akt1 and Akt2 Isoforms—Because Akt1 and Akt2 are the main isoforms expressed in 3T3-L1 adipocytes (17), we next examined the effect of SHIP2 expression on the insulin-induced phosphorylation of Akt1 and Akt2. The cell lysates were immunoprecipitated with anti-Akt1 antibody, and the precipitates were immunoblotted with anti-phosphospecific Akt antibody. As shown in Fig. 4*C*, Akt1 is efficiently immunoprecipitated by this procedure, and the Akt2 isoform is not present in the precipitates. Insulin induced phosphorylation of the Akt1 isoform at Thr^{308} and Ser^{473} in anti-Akt1 immunoprecipitates, and this phosphorylation was not affected by the expression of either WT-SHIP2 or ΔIP-SHIP2 (Fig. 4, *A* and *B*). Because an anti-Akt2 antibody was not available for the immunoprecipitation, we performed an immunodepletion experiment. After the cell lysates were effectively immunoprecipitated with anti-Akt1 antibody, the supernatants were used for the experiment with Akt2. As can be seen in Fig. 4*F*, only Akt2, not Akt1, is present in the sample obtained by this procedure. Importantly, insulin-induced phosphorylation of Akt2 at Thr^{309} and Ser^{474} was markedly decreased by the expression of WT-SHIP2, whereas it was increased by the expression of ΔIP-SHIP2 (Fig. 4, *D* and *E*). These results indicate that SHIP2 regulates the insulin-induced phosphorylation of Akt2, and not Akt1, in 3T3-L1 adipocytes.

Effect of SHIP2 Expression on the Insulin-induced Subcellular Distribution of Akt Isoforms—It is known that growth factor induces a subcellular relocalization of Akt to the plasma membrane to be phosphorylated (10, 20, 25). Although SHIP2 negatively regulates insulin-induced Akt2 phosphorylation, it is unclear whether SHIP2 affects the phosphorylation of Akt directly or via its translocation to the PM. To address this issue, we next examined the effect of SHIP2 expression on the insulin-induced subcellular redistribution of Akt1 and Akt2. The Akt1 isoform mainly resides in the cytosol fraction, and insulin treatment did not appear to induce apparent subcellular redistribution. In addition, overexpression of neither WT-SHIP2 nor ΔIP-SHIP2 appeared to affect the subcellular localization of Akt1 (Fig. 5*A*). Thus, the amount of Akt1 in the cytosol did not significantly alter in response to insulin. The Akt2 isoform is also mainly localized in the cytosol fraction in the basal state. Compared with the results obtained with Akt1, insulin efficiently elicited a subcellular redistribution of the Akt2 isoform from the cytosol and LDM to the PM. Importantly, the redistribution was markedly decreased by the expression of WT-SHIP2, whereas it was enhanced by that of ΔIP-SHIP2 (Fig. 5*B*). These results indicate that SHIP2 appears to regulate the subcellular redistribution of Akt2, and not Akt1, in 3T3-L1 adipocytes.

Insulin-induced Subcellular Redistribution of SHIP2—Our previous study (26) indicated that the membrane localization of SHIP2 is important for its functioning via the 5′-phosphatase activity. Expression of SHIP2 with the myristoylation signal efficiently inhibited insulin-induced phosphorylation of Akt in Rat1 fibroblasts (26). Given this, we reasoned that SHIP2 might elicit this function by changing the subcellular localization to efficiently regulate the phosphorylation of Akt in the PM fraction. We examined whether insulin induces the subcellular redistribution of SHIP2 (Fig. 6*A*). WT-SHIP2 resides largely in the cytosol and partly in the LDM and PM fractions in the basal state. Insulin treatment significantly induced a redistribution of some of the expressed WT-SHIP2 and ΔIP-SHIP2 to the PM fraction. We further assessed the role of PI3-kinase in the insulin-induced redistribution of SHIP2. Pretreatment of the cells with the PI3-kinase inhibitor LY294002 partly, but significantly, inhibited the insulin-induced redistribution of both WT-SHIP2 and ΔIP-SHIP2 to the PM. Densitometric analysis demonstrated that the redistribution of WT-SHIP2 and ΔIP-SHIP2 to the PM was inhibited 41.3 ± 7.2 and 51.7 ± 6.6%, respectively, by treatment with LY294002. A similar degree of inhibition was obtained on treatment with wortmannin (data not shown). To assure that the LY294002 used in the experiment effectively inhibited the PI-kinase activity, the effect of pretreatment on insulin-induced phosphorylation of Akt was examined. Pretreatment with LY294002 effectively inhibited the insulin-induced phosphorylation of Akt (Fig. 6*B*). These results indicate that insulin induces a redistribution of SHIP2 from the cytosol to the PM fraction independent of the 5′-phosphatase activity of SHIP2 and that this redistribution is partly dependent on the PI3-kinase activity.

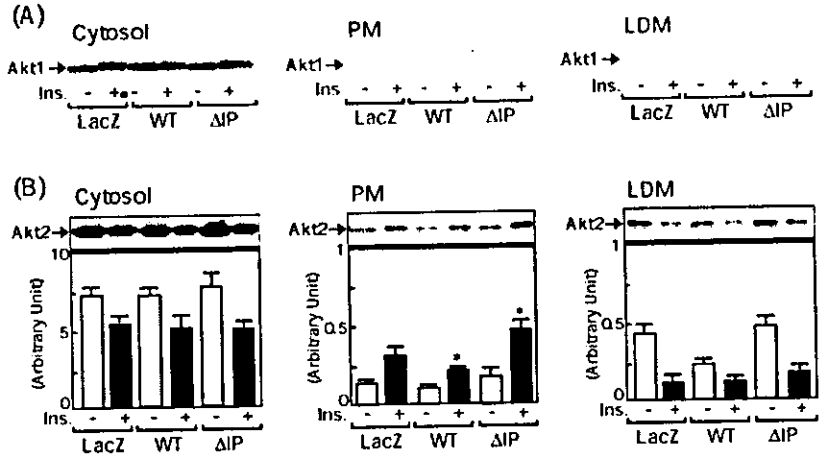

FIG. 5. **Effect of SHIP2 expression on insulin-induced subcellular redistribution of Akt isoforms.** 3T3-L1 adipocytes were transfected with LacZ, WT-SHIP2, or ΔIP-SHIP2 at an m.o.i. of 40 pfu/cell. The cells were serum-starved for 16 h and then treated with 17 nM insulin for 5 min. The cells were homogenized and subjected to subcellular fractionation to yield the cytosol, LDM, and PM fractions. Samples in each fraction were separated by SDS-PAGE and immunoblotted with anti-Akt1 antibody (*A*) or anti-Akt2 antibody (*B*). The amount of Akt2 corrected for the amount loaded was quantitated by densitometry. Results are means ± S.E. of four separate experiments. *, $p < 0.05$ *versus* the amount of Akt after insulin stimulation in LacZ-transfected control cells using the Student's *t* test.

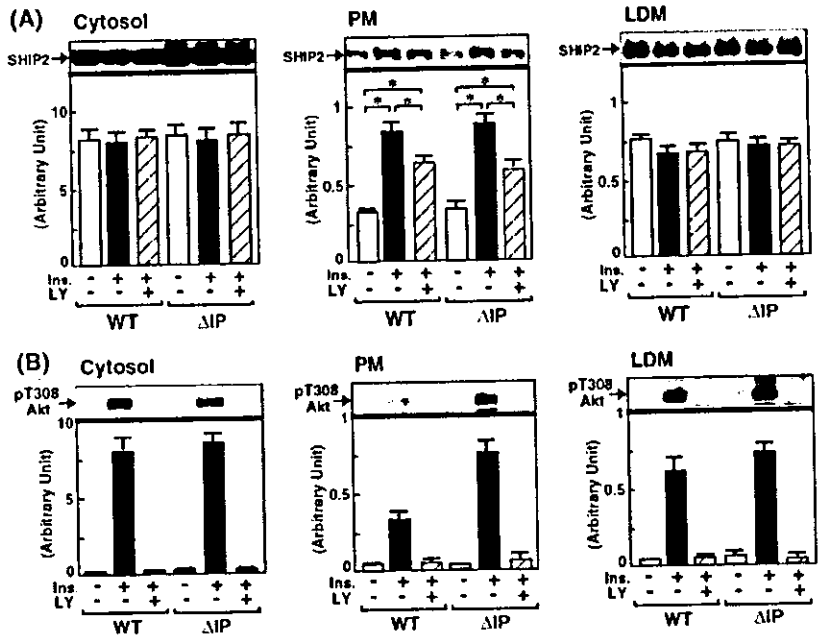

FIG. 6. **Insulin-induced subcellular redistribution of SHIP2 and effect of the PI3-kinase inhibitor LY294002.** 3T3-L1 adipocytes were transfected with either WT-SHIP2 or ΔIP-SHIP2 at an m.o.i. of 40 pfu/cell. The cells were serum-starved for 16 h, incubated with or without 20 μM LY294002 for 30 min, and then treated with 17 nM insulin for 5 min. The cells were homogenized and subjected to subcellular fractionation to yield the cytosol, LDM, and PM fractions. Samples in each fraction were separated by SDS-PAGE and immunoblotted with anti-SHIP2 antibody (*A*) or anti-Thr^{308}-phospho-specific Akt antibody (*B*). The amount of SHIP2 and of Akt phosphorylated at Thr^{308} corrected for the amount of protein loaded was quantitated by densitometry. Results are means ± S.E. of four separate experiments. *, $p < 0.05$, compared by the Student's *t* test.

Effect of SHIP2 Expression on myr-p110-induced Subcellular Distribution and Phosphorylation of Akt—A number of growth factors stimulate PI3-kinase activity in addition to insulin (2, 3). We next examined the effect of SHIP2 expression on the PI3-kinase-induced subcellular distribution and phosphorylation of Akt. To this end, we employed myr-p110, which is a constitutively active from of the catalytic subunit of PI3-kinase (21). Similar to insulin, myr-p110 induced a recruitment of SHIP2 to the PM fraction (Fig. 7*A*). In addition, myr-p110 also induced phosphorylation of Akt at Thr^{308} in the cytosol, PM, and LDM fractions. Similarly, the myr-p110-induced phosphorylation of Akt in the cytosol fraction was apparently not affected by the expression of WT-SHIP2. SHIP2 regulated the insulin-induced phosphorylation of Akt at Thr^{308} in the PM fraction, but the degree to which the myr-p110-induced phosphorylation of Akt was regulated by SHIP2 relatively mild (Fig. 7*B*). Thus, expression of WT-SHIP2 inhibited myr-p110-induced phosphorylation of Akt by 27.3 ± 4.2%. Similar results were obtained concerning the effect of SHIP2 expression on myr-p110-induced phosphorylation of Akt at Ser^{473} (data not shown). Interestingly, the myr-p110-induced redistribution of Akt2 to the PM fraction was not affected by SHIP2 expression (Fig. 7*C*).

Effect of SHIP2 Expression on Insulin-induced Phosphorylation of Akt in Embryonic Fibroblasts Derived from IRS-1 and IRS-2 Knockout Mice—The metabolic action of insulin is mediated via IRS-1 and/or IRS-2 (1, 4, 27–31). Although IRS-1 and IRS-2 have structural similarities, each coordinates, at least in part, different insulin actions (22, 27, 32–34). We further investigated whether IRS-1- and IRS-2-mediated insulin signaling can be regulated by SHIP2. To this end, we employed embryonic fibroblasts derived from IRS-1 and IRS-2 knockout mice (22). Insulin induced the phosphorylation of Akt at Thr^{308} and Ser^{473} in control embryonic fibroblasts expressing both IRS-1 and IRS-2. The phosphorylation of Akt was also seen in IRS-1(−/−) and IRS-2(−/−) embryonic fibroblasts. The insulin-induced phosphorylation of Akt at Thr^{308} and Ser^{473} was decreased by the expression of WT-SHIP2, whereas it was enhanced by the expression of ΔIP-SHIP2 in control, IRS-1(−/−), and IRS-2(−/−) embryonic fibroblasts (Fig. 8, *A* and *B*). These results indicate that SHIP2 is involved in the negative regulation of both IRS-1- and IRS-2-mediated insulin signaling. To assure equal amounts of protein were loaded among the samples, the cell lysates were immunoblotted with anti-Akt antibody. Similar expression levels of WT-SHIP2 and ΔIP-SHIP2

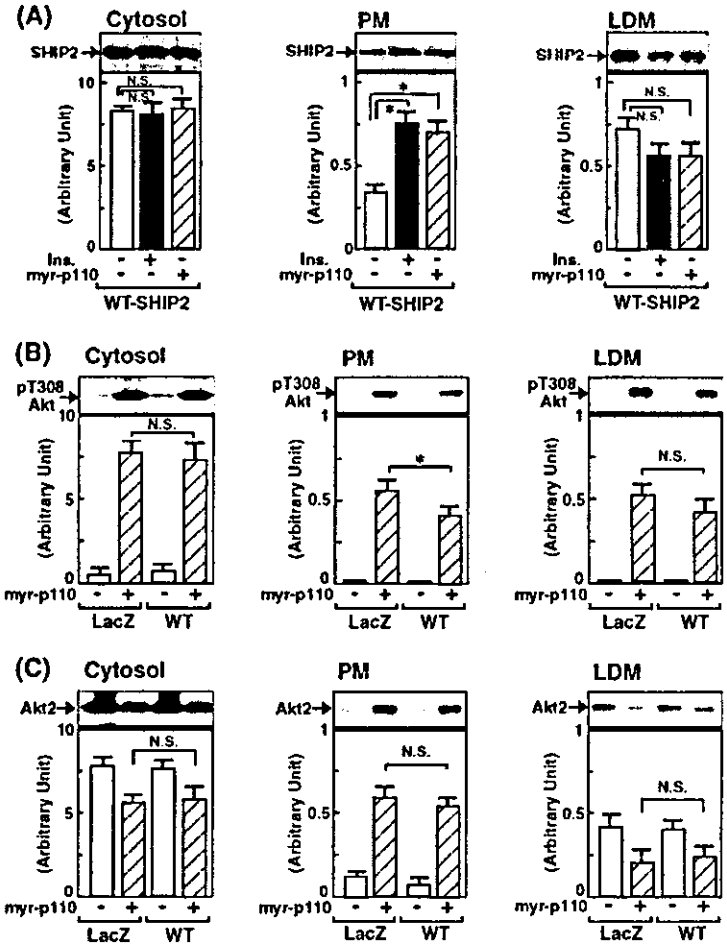

FIG. 7. **Effect of SHIP2 expression on myr-p110-induced subcellular distribution and phosphorylation of Akt.** 3T3-L1 adipocytes were transfected with myr-p110 at an m.o.i. of 40 pfu/cells. The cells were cotransfected with either LacZ or WT-SHIP2 at an m.o.i. of 40 pfu/cell. For the study with insulin treatment, the cells were serum-starved for 16 h and treated with 17 nM insulin for 5 min. The cells were then homogenized and subjected to subcellular fractionation to yield the cytosol, LDM, and PM fractions. Samples in each fraction were separated by SDS-PAGE and immunoblotted with anti-SHIP2 antibody (*A*), anti-Thr^{308}-phosphospecific Akt antibody (*B*), or anti-Akt antibody (*C*). The amount of SHIP2, Akt phosphorylated at Thr^{308}, and Akt protein corrected for the amount loaded was quantitated by densitometry. Results are means ± S.E. of four separate experiments. *, $p < 0.05$, compared by the Student's *t* test.

were confirmed on immunoblotting of the cell lysates with anti-SHIP2 antibody (Fig. 8*C*).

DISCUSSION

The SHIP family is composed of SHIP1 and SHIP2, and overall, the SHIP2 protein exhibits about 40% amino acid identity to SHIP1 (5, 6). Despite their similarities, differences between SHIP1 and SHIP2 have been identified. First, SHIP2 is expressed relatively ubiquitously including in the targets of insulin such as skeletal muscles and fat cells, whereas the expression of SHIP1 is restricted to hematopoietic and spermatogenetic cells (6, 35, 36). Second, these two SHIP isozymes appear to have different substrate specificities. SHIP2 may have greater activity than SHIP1 for the hydrolysis of the PI3-kinase product PI(3,4,5)P_3 (37). These reports suggest that SHIP1 and SHIP2 regulate different inositol-mediated pathways and/or interact differently with effector molecules. Along this line, our previous studies (7, 8) with cultured cells showed that overexpression of SHIP2 negatively regulated insulin-induced metabolic signaling via 5'-phosphatase activity in 3T3-L1 adipocytes and L6 myocytes. Experiments with knockout mice revealed that disruption of SHIP2 expression caused hyperinsulin sensitivity without affecting biological systems other than insulin signaling (9). In addition, the expression of SHIP2 was enhanced leading to an attenuation of insulin signaling distal to PI3-kinase in an animal model of type 2 diabetes (38). Furthermore, mutations in the SHIP2 gene may contribute, at least in part, to the genetic susceptibility to type 2 diabetes in humans (39). Taken together, SHIP2 appears to be a physiologically important negative regulator that is relatively specific to insulin signaling and has a fundamental impact on the pathological state of type 2 diabetes.

To understand the novel control mechanisms in the regulation of insulin signaling by the lipid phosphatase SHIP2, it is important to elucidate how SHIP2 functions following stimulation with insulin. The total 5'-phosphatase activity of SHIP2 is known not to be altered following stimulation with growth factors including insulin (40). Instead, the relocalization of SHIP2 to the vicinity of the plasma membrane would appear to be critical for the functioning based on experiments with SHIP1 (41). Targeting of SHIP2 to the plasma membrane on addition of the myristoylation signal efficiently inhibited the insulin-induced phosphorylation of Akt in Rat1 fibroblasts expressing insulin receptors, although the level of SHIP2 expression in the plasma membrane was low (26). Given this, we reasoned that insulin treatment changes the subcellular relocalization of SHIP2. In fact, insulin induced a redistribution of WT-SHIP2 from the cytosol to the plasma membrane fraction. The insulin-induced localization of SHIP2 to the membrane appears to be critical for the functioning possibly by providing appropriate access to the substrate PI(3,4,5)P_3. In addition, treatment with the PI3-kinase inhibitor LY29004 partly inhibited the insulin-induced redistribution of SHIP2 to the plasma membrane fraction. These results indicate that insulin causes SHIP2 to be redistributed to the plasma membrane where it functions to hydrolyze the PI3-kinase product, and the activation of PI3-kinase itself is required, at least in part, for the

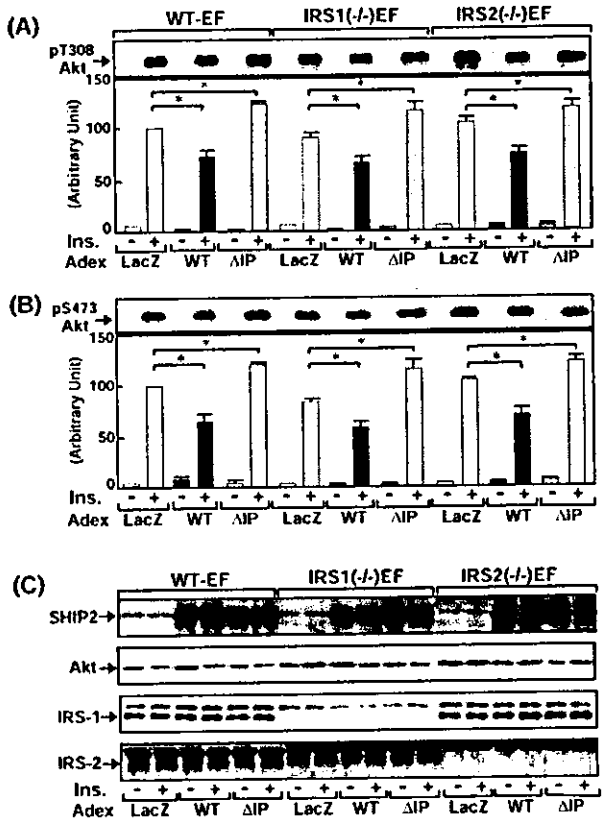

FIG. 8. **Effect of SHIP2 expression on insulin-induced phosphorylation of Akt in embryonic fibroblasts derived from IRS-1 and IRS-2 knockout mice.** Control, IRS-1(−/−), and IRS-2(−/−) embryonic fibroblasts were transfected with LacZ, WT-SHIP2, or ΔIP-SHIP2 at an m.o.i. of 10 pfu/cell. The cells were serum-starved for 16 h and then treated with 17 nM insulin for 5 min. The cell lysates were separated by 7.5% SDS-PAGE and immunoblotted with anti-Thr^{308}-phospho-specific (*A*) or anti-Ser^{473}-phosphospecific (*B*) Akt antibody. *C*, the cell lysates were immunoblotted with anti-SHIP2 antibody, anti-Akt antibody, anti-IRS-1 antibody, or anti-IRS-2 antibody. The amount of Akt phosphorylated at Thr^{308} and Ser^{473} corrected for the amount loaded was quantitated by densitometry. Results are means ± S.E. of four separate experiments. *, $p < 0.05$ *versus* the phosphorylation of Akt after insulin stimulation in LacZ-transfected control cells using the Student's *t* test.

appropriate targeting of SHIP2 to the plasma membrane. It is possible that other signaling molecules, in addition to PI3-kinase, are involved in the subcellular redistribution of SHIP2. Along this line, the association of SHIP2 with Shc appears to be required for the efficient negative regulation of insulin-induced phosphorylation of Akt, at least in part, in Rat1 fibroblasts (26). The association of SHIP2 with Cbl is also reported in Chinese hamster ovary cells (42). Because Shc and Cbl are known to be tyrosine-phosphorylated and undergo a subcellular redistribution to the plasma membrane following insulin stimulation, the tyrosine phosphorylated molecules associated with SHIP2 may have a critical role in the targeting of SHIP2 to the plasma membrane (26, 42). The function of SHIP2 in the negative regulation of insulin signaling remains to be more precisely elucidated.

We have previously reported (7) that SHIP2 inhibits the insulin-induced activation of Akt via 5′-phosphatase activity. The main isoforms of Akt in 3T3-L1 adipocytes are Akt1 and Akt2 (17). Although the two have structural similarities, their physiological roles appear to differ (10, 43–46). Mice with a targeted disruption of Akt1 revealed a defect in growth. However, Akt1-deficient mice are normal with respect to glucose tolerance and insulin-stimulated disposal of blood glucose (43, 44). In contrast, mice lacking Akt2 demonstrated insulin resistance in target tissues of insulin (45, 46). It is also known that Akt2 is abundant in insulin-responsive tissues, and insulin increases the association of Akt2 with Glut4-containing vesicles (10). These results indicate that Akt2 is more important than Akt1 to the metabolic actions of insulin. In this regard, SHIP2 appeared to predominantly regulate the insulin-induced phosphorylation of Akt2, and not Akt1, in 3T3-L1 adipocytes as shown in Fig. 4. Concerning the subcellular localization of Akt, both isoforms were mainly concentrated in the cytosolic fraction of 3T3-L1 adipocytes in the basal state as reported previously (10, 20). Although insulin treatment stimulated phosphorylation of Akt1 in the cytosolic fraction, it did not appear to induce the subcellular redistribution of Akt1. It is of note that, because lesser levels of Akt1 than Akt2 are expressed in differentiated adipocytes (20), lack of the translocation of Akt1 to the plasma membrane may be below the detection limit of our Western blot analysis. In contrast, insulin clearly induced the subcellular redistribution of Akt2 from the cytosol to the plasma membrane fraction and stimulated phosphorylation of Akt2 in all subcellular fractions. The issue of an insulin-induced redistribution of Akt2 to the plasma membrane is controversial, as there is a report that no such redistribution of Akt2 was found in rat fat cells (10). However, our findings are consistent with reports that insulin treatment induces the translocation of Akt2 to the plasma membrane dependent on the PI3-kinase activity in human ovarian cells and 3T3-L1 adipocytes (20, 46, 47). The difference may arise from the experimental conditions used or cells employed among previous reports. Interestingly, the insulin-induced phosphorylation of Akt1 in the cytosolic fraction and the localization of Akt1 did not appear to be affected by the expression of either WT-SHIP2 or ΔIP-SHIP2. In contrast, the insulin-induced phosphorylation of Akt2 was apparently regulated by SHIP2. Furthermore, the degree of inhibition was greater in the plasma membrane fraction than cytosolic fraction. The SHIP2 regulation of Akt phosphorylation and the isoform specificity observed with maximal insulin stimulation (17 nM) appeared to be similarly maintained at a lower concentration of insulin (1.7 nM) stimulation (data not shown). These results indicate that SHIP2 preferentially regulates insulin-induced phosphorylation of Akt2 in the plasma membrane rather than cytosolic fraction. Our results do not rule out the possibility that SHIP2 regulates phosphorylation of Akt2, albeit to a lesser extent, in the cytosolic fraction. It is also possible that the insulin-induced phosphorylation of Akt2 is regulated by SHIP2 exclusively in the plasma membrane fraction, and the weak effect seen in the cytosol fraction was derived from Akt2 returning from the plasma membrane.

Insulin alone can effectively transmit the signaling leading to glucose uptake, although PI3-kinase is activated by a number of growth factors (1–4). Interestingly, platelet-derived growth factor was more effective than insulin in stimulating Akt phosphorylation in fibroblasts, whereas platelet-derived growth factor did not stimulate Akt2 phosphorylation to any significant extent in adipocytes (20). Moreover, insulin, but not platelet-derived growth factor, induced the translocation of Akt2 to the plasma membrane and high density microsome fractions of 3T3-L1 adipocytes (20). These results prompted us to examine the notion of another role for SHIP2, in addition to the regulation of Akt2 phosphorylation, in the control of insulin-induced metabolic signaling. In this regard, we further focused on the part of SHIP2 in the insulin-induced subcellular redistribution of Akt2. Our results showed that SHIP2 regulates myr-p110-induced phosphorylation of Akt mainly in the

plasma membrane fraction. However, the degree of the inhibition was relatively low compared with that for insulin. Furthermore, expression of SHIP2 affected the insulin-induced, and not myr-p110-induced, translocation of Akt2 to the plasma membrane. These results further indicate the molecular mechanism by which SHIP2 relatively specifically regulates insulin-induced metabolic signaling in 3T3-L1 adipocytes.

The insulin-induced activation of PI3-kinase is mediated via insulin receptor substrates (1, 4). Tyrosine-phosphorylated IRS binds to the p85 regulatory subunit of PI3-kinase leading to an activation to generate $PI(3,4,5)P_3$ (1–4). IRS-1 and IRS-2 are the two most ubiquitously expressed members of the IRS family of proteins, which regulates the metabolic actions of insulin (1, 4, 27). Indeed, disruption of the genes for IRS-1 and IRS-2 was shown to result in insulin resistance in mice (27). Although the structures of these two proteins are very similar, targeted disruption of the IRS-1 and IRS-2 gene in mice produced distinct phenotypes (28–31). Some previous studies demonstrated that IRS-1 has a major role in adipocyte differentiation (22, 33). In addition, the IRS-1-PI3-kinase, but not IRS-2-PI3-kinase, pathway was essential for SREBP1c and glucokinase gene expression in rat hepatocytes (32). Furthermore, IRS-2, but not IRS-1, was predominantly involved in Glut4 translocation and glucose uptake in brown adipose tissue (34). Therefore, IRS-1 and IRS-2 regulate the specific biological actions in addition to the redundant metabolic actions of insulin. It is therefore important to clarify whether SHIP2 specifically or non-specifically regulates IRS-1- and IRS-2-mediated insulin signaling. Our results provide direct evidence of a role for SHIP2 in the regulation of IRS-1- and IRS-2-mediated phosphorylation of Akt in IRS-1- or IRS-2-deficient cells. Because the insulin-induced phosphorylation of Akt was similarly regulated by the expression of WT-SHIP2 and ΔIP-SHIP2 among control cells, IRS-1-deficient cells, and IRS-2-deficient cells, SHIP2 appears to have a similar impact on the regulation of insulin signaling by both IRS-1 and IRS-2.

In summary, our results clarified the molecular mechanism by which SHIP2 relatively specifically regulates the metabolic actions of insulin seen in mice with a targeted disruption of SHIP2 (9). First, SHIP2 appears to specifically regulate the metabolic functions of insulin, at least in part, by inhibiting the insulin-induced phosphorylation of Akt2, and not Akt1, in the plasma membrane in 3T3-L1 adipocytes. Second, upon insulin stimulation, SHIP2 is translocated to the plasma membrane, where it inhibits the insulin-specific subcellular redistribution of Akt2. Third, SHIP2 regulates the insulin-induced phosphorylation of Akt mediated via both IRS-1 and IRS-2. Although we clarified the mechanisms of SHIP2 in the regulation of Akt, atypical PKCs including PKCλ and PKCζ are another downstream target of PI3-kinase important for the metabolic actions of insulin. Because the insulin-induced activation of aPKC is also known to be regulated by SHIP2, further study will be required to clarify the molecular mechanism of the regulation of aPKC by SHIP2. Clarification of the novel control mechanisms for insulin could provide a new insight into the development of therapeutic drugs. Thus, inhibition of an endogenous amount and/or function of SHIP2 would be an important therapeutic target of insulin resistance in type 2 diabetes.

Acknowledgments—We thank Dr. Wataru Ogawa (Kobe University) for kindly providing myr-p110. We are grateful to Dr. Atsuko Takano for technical assistance.

REFERENCES

1. Virkamäki, A., Ueki, K., and Kahn, C. R. (1999) *J. Clin. Invest.* **103**, 931–943
2. Cantley, L. C. (2002) *Science* **296**, 1655–1657
3. Rameh, L. E., and Cantley, L. C. (1999) *J. Biol. Chem.* **274**, 8347–8350
4. Czech, M. P., and Corvera, S. (1999) *J. Biol. Chem.* **274**, 1865–1868
5. Ishihara, H., Sasaoka, T., Hori, H., Wada, T., Hirai, H., Haruta, T., Langlois, W. J., and Kobayashi, M. (1999) *Biochem. Biophys. Res. Commun.* **260**, 265–272
6. Pesesse, X., Deleu, S., De Smedt, F., Drayer, L., and Erneux, C. (1997) *Biochem. Biophys. Res. Commun.* **239**, 697–700
7. Wada, T., Sasaoka, T., Funaki, M., Hori, H., Murakami, S., Ishiki, M., Haruta, T., Asano, T., Ogawa, W., Ishihara, H., and Kobayashi, M. (2001) *Mol. Cell Biol.* **21**, 1633–1646
8. Sasaoka, T., Hori, H., Wada, T., Ishiki, M., Haruta, T., Ishihara, H., and Kobayashi, M. (2001) *Diabetologia* **44**, 1258–1267
9. Clement, S., Krause, U., Desmedt, F., Tanti, J. F., Behrends, J., Pesesse, X., Sasaki, T., Penninger, J., Doherty, M., Malaisse, W., Dumont, J. E., Le Marchand-Brustel, Y., Erneux, C., Hue, L., and Schurmans, S. (2001) *Nature* **409**, 92–97
10. Calera, M. R., Martinez, C., Liu, H., El Jack, A. K., Birnbaum, M. J., and Pilch, P. F. (1998) *J. Biol. Chem.* **273**, 7201–7204
11. Kohn, A. D., Summers, S. A., Birnbaum, M. J., and Roth, R. A. (1996) *J. Biol. Chem.* **271**, 31372–31378
12. Cong, L.-N., Chen, H., Li, Y., Zhou, L., McGibbon, M. A., Taylor, S. I., and Quon, M. J. (1997) *Mol. Endocrinol.* **11**, 1881–1890
13. Andjelkovic, M., Alessi, D. R., Meier, R., Fernandez, A., Lamb, N. J. C., Frech, M., Cron, P., Cohen, P., Lucocq, J. M., and Hemmings, B. A. (1997) *J. Biol. Chem.* **272**, 31515–31524
14. Franke, T. F., Kaplan, D. R., Cantley, L. C., and Toker, A. (1997) *Science* **275**, 665–668
15. Stephens, L., Anderson, K., Stokoe, D., Erdjument-Bromage, H., Painter, G. F., Holmes, A. B., Gaffney, P. R. J., Reese, C. B., McCormick, F., Tempst, P., Coadwell, J., and Hawkins, P. T. (1998) *Science* **279**, 710–714
16. Stokoe, D., Stephens, L. R., Copeland, T., Gaffney, P. R. J., Reese, C. B., Painter, G. F., Holmes, A. B., McCormick, F., and Hawkins, P. T. (1997) *Science* **277**, 567–570
17. Katome, T., Obata, T., Matsushima, R., Masuyama, N., Cantley, L. C., Gotoh, Y., Kishi, K., Shiota, H., and Ebina, Y. (2003) *J. Biol. Chem.* **278**, 28312–28323
18. Anai, M., Ono, H., Funaki, M., Fukushima, Y., Inukai, K., Ogihara, T., Sakoda, H., Onishi, Y., Yazaki, Y., Kikuchi, M., Oka, Y., and Asano, T. (1998) *J. Biol. Chem.* **273**, 29686–29692
19. Clark, S. F., Martin, S., Carozzi, A. J., Hill, M. M., and James, D. E. (1998) *J. Cell Biol.* **140**, 1211–1225
20. Hill, M. M., Clark, S. F., Tucker, D. F., Birnbaum, M. J., James, D. E., and Macaulay, S. L. (1999) *Mol. Cell Biol.* **19**, 7771–7781
21. Kitamura, T., Kitamura, Y., Kuroda, S., Hino, Y., Ando, M., Kotani, K., Konishi, H., Matsuzaki, H., Kikkawa, U., Ogawa, W., and Kasuga, M. (1999) *Mol. Cell Biol.* **19**, 6286–6296
22. Miki, H., Yamauchi, T., Suzuki, R., Komeda, K., Tsuchida, A., Kubota, N., Terauchi, Y., Kamon, J., Kaburagi, Y., Matsui, J., Akanuma, Y., Nagai, R., Kimura, S., Tobe, K., and Kadowaki, T. (2001) *Mol. Cell Biol.* **21**, 2521–2532
23. Heller-Harrison, R. A., Morin, M., and Czech, M. P. (1995) *J. Biol. Chem.* **270**, 24442–24450
24. Inoue, G., Cheatham, B., Emkey, R., and Kahn, C. R. (1998) *J. Biol. Chem.* **273**, 11548–11555
25. Scheid, M. P., Marignani, P. A., and Woodgett, J. R. (2002) *Mol. Cell Biol.* **22**, 6247–6260
26. Ishihara, H., Sasaoka, T., Ishiki, M., Wada, T., Hori, H., Kagawa, S., and Kobayashi, M. (2002) *Mol. Endocrinol.* **16**, 2371–2381
27. Kadowaki, T. (2000) *J. Clin. Invest.* **106**, 459–465
28. Tamemoto, H., Kadowaki, T., Tobe, K., Yagi, T., Sakura, H., Hayakawa, T., Terauchi, Y., Ueki, K., Kaburagi, Y., Satoh, S., Sekihara, H., Yoshioka, S., Horikoshi, H., Furuta, Y., Ikawa, Y., Kasuga, M., Yazuki, Y., and Aizawa, S. (1994) *Nature* **372**, 182–186
29. Araki, E., Lipes, M. A., Patti, M. E., Brüning, J. C., Haag, I. B., Johnson, R. S., and Kahn C. R. (1994) *Nature* **372**, 186–190
30. Withers, D. J., Gutierrez, J. S., Towery, H., Burks, D. J., Ren, J.-M., Previs, S., Zhang, Y., Bernal, D., Pons, S., Shulman, G. I., Bonner-Weir, S., and White, M. F. (1998) *Nature* **391**, 900–904
31. Kubota, N., Tobe, K., Terauchi, Y., Eto, K., Yamauchi, T., Suzuki, R., Tsubamoto, Y., Komeda, K., Nakano, R., Miki, H., Satoh, S., Sekihara, H., Sciacchitano, S., Lesniak, M., Aizawa, S., Nagai, R., Kimura, S., Akanuma, Y., Taylor, S. I., and Kadowaki, T. (2000) *Diabetes* **49**, 1880–1889
32. Matsumoto, M., Ogawa, W., Teshigawara, K., Inoue, H., Miyake, K., Sakaue, H., and Kasuga, M. (2002) *Diabetes* **51**, 1672–1680
33. Fasshauer, M., Klein, J., Kriauciunas, K. M., Ueki, K., Benito, M., and Kahn, C. R. (2001) *Mol. Cell Biol.* **21**, 319–329
34. Fasshauer, M., Klein, J., Ueki, K., Kriauciunas, K. M., Benito, M., White, M. F., and Kahn, C. R. (2000) *J. Biol. Chem.* **275**, 25494–25501
35. Osborne, M. A., Zenner, G., Lubinus, M., Zhang, X., Songyang, Z., Cantley, L. C., Majerus, P., Burn, P., and Kochan, J. P. (1996) *J. Biol. Chem.* **271**, 29271–29278
36. Liu, Q., Shalaby, F., Jones, J., Bouchard, D., and Dumont, D. J. (1998) *Blood* **91**, 2753–2759
37. Wisniewski, D., Strife, A., Swendeman, S., Erdjument-Bromage, H., Geromanos, S., Kavanaugh, W. M., Tempst, P., and Clarkson, B. (1999) *Blood* **93**, 2707–2720
38. Hori, H., Sasaoka, T., Ishihara, H., Wada, T., Murakami, S., Ishiki, M., and Kobayashi, M. (2002) *Diabetes* **51**, 2387–2394
39. Marion, E., Kaisaki, P. J., Pouillon, V., Gueydan, C., Levy, J. C., Bodson, A., Krzentowski, G., Daubresse, J.-C., Mockel, J., Behrends, J., Servais, G., Szpirer, C., Kruys, V., Gauguier, D., and Schurmans, S. (2002) *Diabetes* **51**, 2012–2017
40. Habib, T., Hejna, J. A., Moses, R. E., and Decker, S. J. (1998) *J. Biol. Chem.* **273**, 18605–18609
41. Phee, H., Jacob, A., and Coggeshall, K. M. (2000) *J. Biol. Chem.* **275**, 19090–19097
42. Vandenbroere, I., Paternotte, N., Dumont, J. E., Erneux, C., and Pirson, I.

(2003) *Biochem. Biophys. Res. Commun.* **300**, 494–500
43. Chen, W. S., Xu, P.-Z., Gottlob, K., Chen, M.-L., Sokol, K., Shiyanova, T., Roninson, I., Weng, W., Suzuki, R., Tobe, K., Kadowaki, T., and Hay, N. (2001) *Genes Dev.* **15**, 2203–2208
44. Cho, H., Thorvaldsen, J. L., Chu, Q., Feng, F., and Birnbaum, M. J. (2001) *J. Biol. Chem.* **276**, 38349–38352
45. Cho, H., Mu, J., Kim, J. K., Thorvaldsen, J. L., Chu, Q., Crenshaw, E. B., III, Kaestner, K. H., Bartolomei, M. S., Shulman, G. I., and Birnbaum, M. J. (2001) *Science* **292**, 1728–1731
46. Garofalo, R. S., Orena, S. J., Rafidi, K., Torchia, A. J., Stock, J. L., Hildebrandt, A. L., Coskran, T., Black, S. C., Brees, D. J., Wicks, J. R., McNeish, J. D., and Coleman, K. G. (2003) *J. Clin. Invest.* **112**, 197–208
47. Mitsuuchi, Y., Johnson, S. W., Moonblatt, S., and Testa, J. R. (1998) *J. Cell Biochem.* **70**, 433–441

Journal of Neurochemistry, 2004, 89, 1454–1461 doi:10.1111/j.1471-4159.2004.02437.x

Blood-to-retina transport of creatine via creatine transporter (CRT) at the rat inner blood–retinal barrier

Toshihisa Nakashima,* Masatoshi Tomi,*,† Kazunori Katayama,* Masanori Tachikawa,‡ Masahiko Watanabe,§ Tetsuya Terasaki†,‡,¶ and Ken-ichi Hosoya*,†

*Faculty of Pharmaceutical Sciences, Toyama Medical and Pharmaceutical University, Toyama, Japan

†CREST of Japan Science and Technology Corporation (JST), Japan

‡Department of Molecular Biopharmacy and Genetics, Graduate School of Pharmaceutical Sciences and ¶New Industry Creation Hatchery Center, Tohoku University, Sendai, Japan

§Department of Anatomy, Hokkaido University School of Medicine, Sapporo, Japan

Abstract

The purpose of this study was to elucidate the mechanisms of blood-to-retina creatine transport across the blood–retinal barrier (BRB) *in vivo* and *in vitro*, and to identify the responsible transporter(s). The creatine transport across the BRB *in vivo* and creatine uptake in an *in vitro* model of the inner BRB (TR-iBRB2 cells) were examined using [^{14}C]creatine. Identification and localization of the creatine transporter (CRT) were carried out by RT-PCR, western blot, and immunoperoxidase electron microscopic analyses. An *in vivo* intravenous administration study suggested that [^{14}C]creatine is transported from the blood to the retina against the creatine concentration gradient that exists between the retina and blood. [^{14}C]Creatine uptake by TR-iBRB2 cells was saturable, Na^+- and Cl^--dependent and inhibited by CRT inhibitors, suggesting that CRT is involved in creatine transport at the inner BRB. RT-PCR and western blot analyses demonstrated that CRT is expressed in rat retina and TR-iBRB2 cells. Moreover, using an immunoperoxidase electron microscopic analysis, CRT immunoreactivity was found at both the luminal and abluminal membranes of the rat retinal capillary endothelial cells. In conclusion, CRT is expressed at the inner BRB and plays a role in blood-to-retina creatine transport across the inner BRB.

Keywords: blood–retinal barrier, carrier-mediated transport, creatine, creatine transporter, retinal capillary endothelial cells.

J. Neurochem. (2004) **89**, 1454–1461.

Creatine plays an essential role in the storage and transmission of phosphate-bound energy due to the conversion of creatine to phosphocreatine catalyzed by creatine kinase. Creatine would therefore be present at a high concentration in cellular ATP homeostasis, particularly in tissues subject to high metabolic demands, such as the retina, brain, heart, and muscle (Wyss and Kaddurah-Daouk 2000). Although there is no published study of the creatine concentration in the mammalian retina, it has been reported to be 10–15 mM in chicken photoreceptors (Wallimann *et al.* 1986). Therefore, it is hypothesized that the creatine concentration in the mammalian retina is at least a 2-log scale order of magnitude greater than that in plasma, since the plasma creatine concentration is 50–100 μM in humans (Marescau *et al.* 1986; Harris *et al.* 1992) and 140–600 μM in rats (Fitch and Shields 1966; Horn *et al.* 1998). To maintain a high concentration of creatine in the retina, the blood–retinal barrier (BRB) may regulate creatine movement between the circulating blood and the neural retina.

Creatine is biosynthesized mainly in the kidney and liver in two steps by L-arginine:glycine amidinotransferase

Received October 6, 2003; revised manuscript received January 14, 2004; accepted February 9, 2004.

Address correspondence and reprint requests to Ken-ichi Hosoya, Faculty of Pharmaceutical Sciences, Toyama Medical and Pharmaceutical University, 2630, Sugitani, Toyama, 930-0194, Japan.
E-mail: hosoyak@ms.toyama-mpu.ac.jp

Abbreviations used: AGAT, L-arginine:glycine amidinotransferase; BBB, blood–brain barrier; BRB, blood–retinal barrier; CL_{retina}, the apparent influx permeability clearance of retina; CRT, creatine transporter; GA, gyrate atrophy; GAMT, *S*-adenosylmethionine:guanidinoacetate *N*-methyltransferase; inner BRB, inner blood–retinal barrier; $K_{p,app}(t)$, the apparent tissue-to-plasma concentration ratio; RPE, (outer BRB), retinal pigmented epithelial cells; TR-iBRB2, conditionally immortalized rat retinal capillary endothelial cell line.

(AGAT) and *S*-adenosylmethionine:guanidinoacetate *N*-methyltransferase (GAMT) from L-arginine and glycine, and also absorbed from the diet via the intestine (Walker 1979). Mardashchev (1975) reported that GAMT activity is present in the rat, rabbit, bovine, and hen retina. Nevertheless, there is no report of the measurement of AGAT activity in the retina and so it is not known whether creatine is biosynthesized in the retina. Although the creatine transporter (CRT) in muscle and heart plays a role in transporting creatine from the circulating blood (Murphy *et al.* 2001; Boehm *et al.* 2003), there are few direct studies of creatine transport at the BRB.

The BRB, which is composed of retinal capillary endothelial cells (inner BRB) and retinal pigmented epithelial cells (RPE, outer BRB), plays a key role in restricting the non-specific transport of hydrophilic compounds and facilitating the influx and efflux transport of essential molecules and xenobiotics, respectively, from the circulating blood to the retina and vice versa (Cunha-Vaz 1976). Using *in situ* hybridization and northern blot analyses (Jones 1995; Saltarelli *et al.* 1996), CRT mRNA has been shown to be expressed in the bovine and rat retina, respectively; however, our knowledge of the transport mechanism for creatine at the BRB is still incomplete. We recently found that creatine is transported via CRT at the mouse blood–brain barrier (BBB) and even the brain appears to have its own mechanism of creatine synthesis (Defalco and Davies 1961; Braissant *et al.* 2001; Ohtsuki *et al.* 2002). We hypothesize that the BRB plays a role in supplying creatine to the retina from the circulating blood even if creatine can be biosynthesized in the retina. Creatine supplementation has been shown to be beneficial in animal models of amyotrophic lateral sclerosis, Parkinson's disease, and Huntington's disease (Matthews *et al.* 1998, 1999; Klivenyi *et al.* 1999). Gyrate atrophy (GA) of the choroid and retina with hyperornithinemia results in high ornithine and low creatine concentrations in body fluids and leads to chorioretinal degeneration (Sipila *et al.* 1992). In GA patients, however, the effect of creatine supplementation on the progression of eye symptoms appears to be small compared with the skeletal muscles (Vannas-Sulonen *et al.* 1985). Consequently, it is important to elucidate the blood-to-retina transport mechanism(s) of creatine at the BRB as far as the supply of creatine to the neural retina is concerned.

We report here evidence supporting the hypothesis that creatine in the retina is transported from the circulating blood across the BRB. The characteristics and functions of creatine transport at the BRB were examined by *in vivo* integration plot analysis and an *in vitro* model of the inner BRB. The identification of the creatine transporter was performed by RT-PCR and western blot analyses and the localization of CRT at the inner BRB was determined by immunoperoxidase electron microscopic analysis.

Materials and methods

Animals

Male Wistar rats (250–300 g) and male ddY mice (25–30 g) were purchased from SLC (Shizuoka, Japan). The investigations using rats and mice described in this report conformed to the provisions of the Animal Care Committee, Toyama Medical & Pharmaceutical University (# 2002–37) and the ARVO Statement on the Use of Animals in Ophthalmic and Vision Research.

Determination of influx permeability clearance of [^{14}C]creatine *in vivo*

The rats were anesthetized with an intramuscular injection of ketamine–xylazine (1.22 mg xylazine and 125 mg ketamine/kg) and then [4–^{14}C]creatine ([^{14}C]creatine, 55 mCi/mmol, American Radiolabeled Chemicals, St. Louis, MO, USA) (6 μCi/head) was injected via the femoral vein. Tissue sampling and determination of radioactivity were performed according to a previous report (Ohtsuki *et al.* 2002). The apparent influx permeability clearance (CL) of [^{14}C]creatine in the retina (CL_{retina}) [μL/(min·g retina)] was determined by integration plot analysis (Yang *et al.* 1997; Ohtsuki *et al.* 2002). As an index of the tissue distribution characteristics of each compound, the apparent tissue-to-plasma concentration ratio ($K_{p,app}$) was used. This ratio [$K_{p,app}(t)$] (mL/g tissue) was defined as the amount of [^{14}C] per gram tissue divided by that per milliliter plasma, calculated over the time-period of the experiment. In brief, the tissue uptake rate of [^{14}C]creatine can be described by eqn 1:

$$K_{p,app}(t) = CL_{retina} \times AUC(t)/Cp(t) + V_i \quad (1)$$

where $Cp(t)$ (dpm/mL) and V_i (mL/g tissue) represent the plasma concentration at time t and the rapidly equilibrated distribution volume of [^{14}C]creatine, respectively; $AUC(t)$ (dpm·min/mL) is the area under the plasma concentration time curve of [^{14}C]creatine from time 0 to t.

HPLC analysis

The metabolism of [^{14}C]creatine in the retina after intravenous injection was determined by HPLC according to a previous report (Ohtsuki *et al.* 2002). Briefly, the retinas and plasma were collected 15 min after intravenous injection of [^{14}C]creatine (24 μCi/400 μL saline). The samples were treated and subjected to HPLC using a system equipped with a 4.6 mm × 150 mm Inertsil ODS-3™ column (GL Sciences, Tokyo, Japan).

[^{14}C]Creatine uptake by TR-iBRB2 cells

The conditionally immortalized rat retinal capillary endothelial cell line (TR-iBRB2), which had been established and characterized previously (Hosoya *et al.* 2001a,b; Tomi *et al.* 2002), was used as an *in vitro* model of the inner BRB to characterize the creatine transport. The net transendothelial electrical resistance of TR-iBRB2 cells grown on a filter was approximately 30 ohm·cm^2. Therefore, the creatine transport mechanism was evaluated in an uptake study rather than in a transcelluar study. TR-iBRB2 cells (passage number 27–38) were cultured at 33°C in Dulbecco's modified Eagle's medium (Nissui Pharmaceutical Co., Tokyo, Japan) under 5% CO_2/air as described previously (Hosoya *et al.* 2001b). For the uptake study, cells (5×10^4 cells/cm^2) were cultured at 33°C for 2 days on a rat tail collagen type I-coated 24-well plate (BD Biosciences, San

Jose, CA, USA). The uptake procedure and determination of radioactivity in the cells were performed according to previous reports (Ohtsuki *et al.* 2002; Tomi *et al.* 2002). For the concentration-dependent study, a concentration range of creatine from 1.7 μM to 150 μM was prepared using [^{14}C]creatine from 18.7 nCi to 1.65 μCi.

RT-PCR analysis

Total cellular RNA was prepared from phosphate-buffered saline-washed cells using the RNeasy Mini Kit (Qiagen, Hilden, Germany). Single-strand cDNA was made from 1 μg total RNA by reverse transcription using oligo dT primer. The PCR was performed using a gene amplification system (GeneAmp PCR system 9700; PE-Applied Biosystems, Foster City, CA, USA) with creatine transporter through 35 cycles of 94°C for 30 s, 65°C for 1 min, and 72°C for 1 min. The sequences of the specific primers were as follows: the sense sequence was 5′-GAAATGGTGCTG-GTCCTTCTTCAC-3′ and the antisense sequence was 5′-GTCA-CATGACACTCTCCACCACGA-3′ for rat CRT (Slc6a8, GenBank Accession no. X66494). The PCR products were separated by electrophoresis on an agarose gel in the presence of ethidium bromide and visualized under ultraviolet light. The molecular identity of the resultant product was confirmed by a sequence analysis using a DNA sequencer (ABI PRISM 310; PE-Applied Biosystems).

Immunocytochemical study of CRT transfected HEK293 cells

Anti-mouse CRT antibody was raised against amino acid residues 578–635 of mouse CRT (GenBank Accession no. AB077327), which are identical to rat CRT as described previously (Ohtsuki *et al.* 2002). For the rat CRT expression in HEK293 cells, an open reading frame subcloned into IRES-neo vector (BD Biosciences) was used. PCR was performed with KOD DNA polymerase (Toyobo, Osaka, Japan) using primer sets: rat CRT sense primers, 5′-CACCCTCGAGACGCCGCGAC-3′ and antisense primer, 5′-AGGATGAGCTGGTGATGTGAGCT-3′. HEK293 cells were cultured at 37°C in an atmosphere of 5% CO_2/air in minimum essential medium (Invitrogen, Carlsbad, CA, USA) supplemented with 2.2 g/L sodium bicarbonate, 100 U/mL penicillin, 100 μg/mL streptomycin, and 10% fetal bovine serum. For transfection, 1×10^5 HEK293 cells were seeded on 24-well plates (BD Biosciences). After 24 h cultivation, cells were transfected using a complex of 98 μL OPTI-MEM I (Invitrogen), 2 μL LIPOFECTAMINE 2000 reagent (Invitrogen) and 0.8 μg of the indicated plasmid. After 48 h, transfected cells were fixed in 4% paraformaldehyde/0.1 M sodium phosphate buffer (pH 7.2). After incubating in MeOH : acetic acid solution (90 : 5) for 10 min at −20°C, cells were reacted with rabbit anti-mouse CRT antibody (2 μg/mL) in 1% bovine serum albumin for 16 h at 4°C, and then with FITC-conjugated donkey anti-rabbit IgG (1 : 50 dilution) in 1% bovine serum albumin for 2 h at room temperature. Cells were viewed under a fluorescence microscope (IX70, Olympus, Tokyo, Japan).

Western blot analysis

Tissue and cell lysates of mouse brain, rat brain, rat retina, and TR-iBRB2 cells were prepared in buffer containing 50 mM Tris-HCl, 25 mM KCl, 250 mM sucrose, 1 mM $MgCl_2 \cdot 6H_2O$, and a protease-inhibitor cocktail (Sigma, St. Louis, MO, USA). Preparation of crude membrane fractions and western blot analysis were performed according to a previous report (Ohtsuki *et al.* 2002).

Immunoperoxidase electron microscopic analysis

Under deep pentobarbital anesthesia (100 mg/kg body weight, i.p.), Wistar rats were perfused transcardially with 4% paraformaldehyde in 0.1 M sodium phosphate buffer (pH 7.2). Microslicer sections through the retina (100 μm in thickness, VT1000S; Leica, Nussloch, Germany) were subjected to immunoperoxidase using a Histofine SAB-PO(R) kit (Nichirei, Tokyo, Japan). Sections were incubated at room temperature with 10% normal goat serum for 20 min, rabbit anti-mouse CRT antibody (2 μg/mL) overnight, biotinylated goat anti-rabbit IgG for 2 h, and streptavidin–peroxidase complex for 30 min, followed by visualization with 3,3′-diaminobenzidine. Sections were further treated with 1% osmium tetraoxide for 15 min, 2% uranyl acetate for 60 min, dehydrated using graded alcohol concentrations, and embedded in Epon 812. Electron micrographs were taken with an H7100 electron microscope (Hitachi, Tokyo, Japan).

Data analysis

The uptake of [^{14}C]creatine by TR-iBRB2 cells was expressed as the cell-to-medium (cell/medium) ratio according to previous reports (Ohtsuki *et al.* 2002; Tomi *et al.* 2002). The [^{3}H]D-mannitol (17 Ci/mmol, PerkinElmer Life Sciences, Boston, MA, USA) uptake study was performed to estimate the volume of adhering water. The resulting cell/medium ratio was 0.1–0.2 μL/mg protein and > 10-fold lower than that of [^{14}C]creatine. Therefore, adhering water was ignored when calculating the cell/medium ratio.

For kinetic studies, the Michaelis constant (K_m) and the maximal rate (J_{max}) of creatine uptake were calculated from the following equation (eqn 2) using the non-linear least-square regression analysis program, MULTI (Yamaoka *et al.* 1981).

$$J = J_{max} \times [S]/(K_m + [S]) \quad (2)$$

where J and [S] are the uptake rate of creatine at 10 min and the concentration of creatine, respectively.

Unless otherwise indicated, all data represent means ± SEM. Statistical significance of differences among means of several groups was determined by one-way analysis of variance (ANOVA) followed by modified Fisher's least squares difference method.

Results

Blood-to-retina transport of creatine across the BRB

The *in vivo* blood-to-retina influx transport of creatine from the circulating blood to the retina through the BRB was evaluated by integration plot analysis after intravenous administration of [^{14}C]creatine to rats (Fig. 1a). The CL_{retina} of [^{14}C]creatine was determined to be 10.7 ± 3.8 μL/(min·g retina) from the slope representing the apparent influx permeability clearance across the BRB using eqn 1. In order to compare the tissue distribution of [^{14}C]creatine, the tissue accumulation of creatine at 15 min and 2 h was examined in the retina, brain, skeletal muscle, and heart (Fig. 1b). The

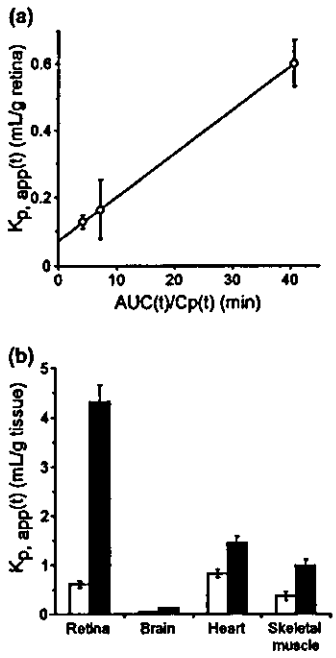

Fig. 1 Blood-to-retina transport of creatine. (a) Integration plot analysis of the initial uptake of [^{14}C]creatine by the retina after intravenous administration. [^{14}C]Creatine (6 μCi/head) was injected via the femoral vein. The apparent influx permeability clearance of [^{14}C]creatine per gram retina (CL_{retina}) was determined to be 10.7 ± 3.8 μL/(min·g retina), calculated from the slope of $K_{p,app}(t)$ vs. AUC(t)/Cp(t) plot. Each point represents the mean ± SEM (n = 3–5). (b) The apparent tissue-to-plasma concentration [$K_{p,app}(t)$] of [^{14}C]creatine was determined 15 min (open column) and 2 h (closed column) after intravenous administration (6 μCi/head). Each column represents the mean ± SEM (n = 3–5).

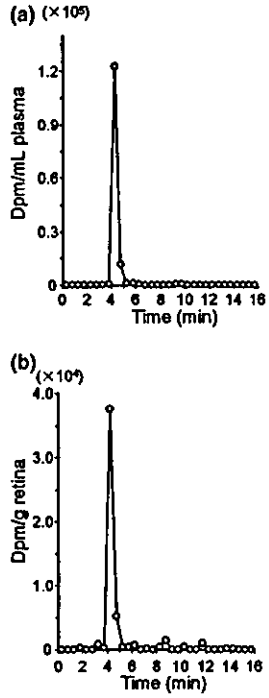

Fig. 2 Typical HPLC chromatogram of samples of plasma (a) and retina (b) after intravenous administration of [^{14}C]creatine. [^{14}C]Creatine (24 μCi/head)was injected via the femoral vein and retinas and plasma were collected at 15 min.

apparent tissue-to-plasma concentration ratio, $K_{p,app}(t)$, of the retina at 15 min and 2 h was 0.603 ± 0.070 and 4.31 ± 0.26 mL/g retina, respectively. The $K_{p,app}(t)$, of the brain, heart, and skeletal muscle at 2 h was 0.127 ± 0.009, 1.45 ± 0.14, and 0.991 ± 0.113 mL/g tissue, respectively. The values of $K_{p,app}(t)$, for the retina were significantly greater than the apparent luminal volume of the retinal capillaries. The y intercept of the integration plot (V_i) value was 0.0763 mL/g tissue (Fig. 1a) and the $K_{p,app}(t)$ for the retina determined at 15 min by [^{3}H]D-mannitol, which is used as a non-permeable paracellular marker, was 0.0575 ± 0.0017 mL/g tissue (n = 4). These values correspond to the apparent luminal volume of the retinal capillaries. HPLC analysis revealed that over 85% of the recovered [^{14}C] activity in plasma and retina was detected at the same retention time as creatine and no metabolites were detected 15 min after intravenous administration (Figs 2a and b). These results demonstrate that creatine is transported in unchanged form from the blood to the retina across the BRB.

Characterization of creatine transport

In order to elucidate the transport mechanism of creatine, TR-iBRB2 cells were used as an *in vitro* model of the rat inner BRB. The [^{14}C]creatine uptake by TR-iBRB2 cells exhibited a time-dependent increase for at least 30 min and reached a cell/medium ratio of 45.5 ± 3.3 μL/mg protein at 30 min (Fig. 3a). In contrast, the absence of either Na^+ or Cl^- reduced the [^{14}C]creatine uptake by more than 80% (Fig. 3b), supporting the hypothesis that creatine uptake by TR-iBRB2 cells takes place in an Na^+- and Cl^--dependent manner. Figure 4 shows the concentration-dependent [^{14}C]creatine uptake by TR-iBRB2 cells. The Eadie–Scatchard plot (Fig. 4, inset) gave a single straight line, indicating that one saturable process was involved in creatine uptake by TR-iBRB2 cells. Kinetic analysis of the uptake data using eqn 2 by non-linear least-squares regression analysis, yielded a K_m of 14.9 ± 1.3 μM and a J_{max} of 49.3 ± 1.7 pmol/(min·mg protein) (mean ± SD). The inhibition study was performed to characterize the [^{14}C]creatine uptake by TR-iBRB2 cells (Table 1). β-Guanidinopropionate and γ-guanidinobutyrate, potent inhibitors of CRT (Möller and Hamprecht. 1989; Sora *et al.* 1994), markedly inhibited [^{14}C]creatine uptake by 91.3% and 72.3%, respectively, whereas phosphocreatine had a weaker effect and creatinine, L-arginine, and

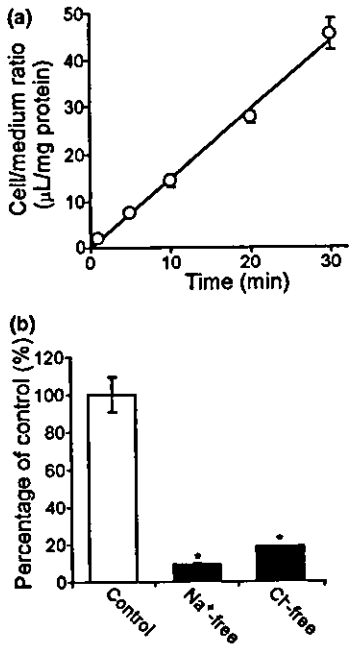

Fig. 3 Time-course of [^{14}C]creatine uptake (a) and Na^+- and Cl^--dependence of [^{14}C]creatine uptake by TR-iBRB2 cells (b). [^{14}C]Creatine uptake (0.2 μCi, 18.2 μM) by TR-iBRB2 cells was performed in the presence (control) or absence of Na^+ and Cl^- (Na^+ and Cl^- were replaced with equimolar Li^+ and gluconate, respectively) at 5 min and 37°C. The uptake was expressed as the cell/medium ratio. Each point and column represents the mean ± SEM (n = 4).

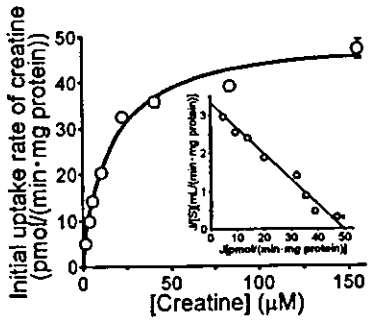

Fig. 4 Concentration-dependence of creatine uptake by TR-iBRB2 cells. [^{14}C]Creatine uptake by TR-iBRB2 cells was performed at 10 min and 37°C, over the concentration range 1.7 μM (18.7 nCi) to 150 μM (1.65 μCi). Each point represents the mean ± SEM (n = 4). The inset graph shows the Eadie–Scatchard plot. Solid lines were fitted using the non-linear least-squares regression analysis program. Using eqn 2, the K_m and J_{max} values were found to be 14.9 ± 1.3 μM and 49.3 ± 1.7 pmol/(min·mg protein), respectively (mean ± SD).

γ-aminobutyric acid (GABA) had no significant effect. This type of inhibition of [^{14}C]creatine uptake suggests that CRT is involved in the uptake process by TR-iBRB2 cells.

Table 1 Effect of several compounds on [^{14}C]creatine uptake by TR-iBRB2 cells

Inhibitors	Percentage of control (%)
Control	100 ± 2
Creatine	5.97 ± 0.56*
β-Guanidinopropionate	8.74 ± 1.01*
γ-Guanidinobutyrate	27.7 ± 3.0*
Phosphocreatine	57.7 ± 3.2*
Creatinine	91.1 ± 1.9
L-Arginine	86.1 ± 3.9
GABA	93.9 ± 2.2

[^{14}C]Creatine uptake (18.2 μM) by TR-iBRB2 cells was performed in the absence (control) or presence of 1 mM inhibitors at 10 min and 37°C. Each value represents the mean ± SEM (n = 4).
* $p < 0.01$, significantly different from control.

Expression and localization of creatine transporter

To determine the CRT expression in rat retina and TR-iBRB2 cells, RT-PCR analysis was performed using total RNA isolated from TR-iBRB2 cells, rat retina, rat brain, and rat skeletal muscle as positive controls for CRT and a specific primer set of rat CRT (Fig. 5a). CRT mRNA was amplified at 353 bp in TR-iBRB2 cells, rat retina, brain, and skeletal muscle. The anti-mouse CRT antibody was raised against amino acid residues 578–635 of mouse CRT as described previously (Ohtsuki *et al.* 2002). Although amino acid residues 578–635 of mouse CRT are identical to rat CRT, we examined CRT immunoreactivity for anti-mouse CRT antibody using rat CRT transfected HEK293 cells (Fig. 5b). Immunoreactivity was observed in rat CRT transfected HEK293 cells (Fig. 5bi), but not in vector transfected HEK293 cells (Fig. 5biii), supporting the hypothesis that anti-mouse CRT antibody can react with rat CRT. Western blot analysis with anti-mouse CRT antibody was conducted using total protein of mouse brain, rat brain and rat retina, and crude membrane of rat brain and TR-iBRB2 cells (Fig. 5c). Bands at 85 kDa and 71 kDa, which were detected in all samples, show that CRT is expressed in rat retina and TR-iBRB2 cells. The localization of CRT was determined in rat retinal capillary endothelial cells by immunoperoxidase electron microscopic analysis (Fig. 6). Immunoreaction products for CRT were detected at high concentrations in the luminal and abluminal membranes of the retinal capillary endothelial cells. The CRT immunoreactivity at the abluminal membrane tended to be greater than that at the luminal membrane. These features indicate that CRT is expressed at the luminal and abluminal membranes of rat retinal capillary endothelial cells.

Discussion

The present study demonstrates, for the first time, that creatine is transported from the circulating blood to the retina

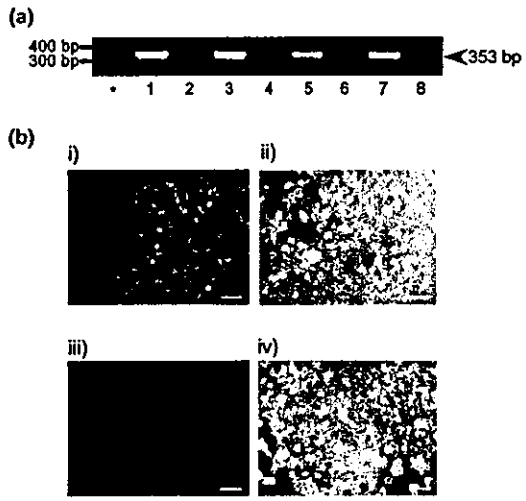

Fig. 5 Expression of creatine transporter mRNA and protein in rat retina and TR-iBRB cells. (a) RT-PCR analysis of rat CRT mRNA. Lane 1, rat skeletal muscle; lane 3, rat brain; lane 5, rat retina; lane 7, TR-iBRB2 cells. Lanes 2, 4, 6, and 8 are in the absence of reverse transcriptase for each left-hand side lane. Rat skeletal muscle and brain were used as positive controls. (b) Immunocytochemical analysis of rat CRT-transfected HEK293 cells with anti-mouse CRT antibody. The immunoreactivity was examined in HEK293 cells transfected with rat CRT (i) and vector alone (iii) after incubation of FITC-conjugated donkey anti-rabbit IgG. The phase-contrast images (ii and iv) correspond to left-hand fields (i and iii). Scale bar: 100 μm. (c) Western blot analysis of rat CRT protein in retina and TR-iBRB2 cells. Lane 1, total protein of adult mouse brain; lane 2, total protein of adult rat brain; lane 3, total protein of adult rat retina; lane 4, crude membrane fraction of adult rat brain; lane 5, crude membrane fraction of TR-iBRB2 cells. Mouse and rat brain were used as positive controls. The DNA and protein size makers are indicated on the left-hand side (a, c).

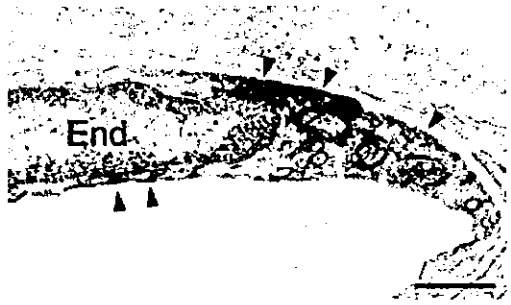

Fig. 6 Localization of creatine transporter in rat retinal capillary endothelial cells. Immunoperoxidase electron microscopy of CRT in rat retinal capillary endothelial cells. Immunoperoxidase labeling (arrowheads) was detected on the surface of both luminal and abluminal membranes of rat retinal capillary endothelial cells (End). Scale bar: 0.5 μm.

across the BRB and that CRT is expressed and localized in retinal capillary endothelial cells. The characteristics of [^{14}C]creatine uptake by TR-iBRB2 cells used as an *in vitro* model of the inner BRB support the belief that CRT is involved in creatine transport at the inner BRB. Creatine was transported from the blood to the retina across the BRB and accumulated in unchanged form in the retina with a CL_{retina} of 10.7 μL/(min·g retina) (Figs 1 and 2). This figure is approximately 20-fold greater than that of [^{14}C]sucrose [approximately 0.5 μL/(min·g retina)] used as a non-permeable paracellular marker (Ennis and Betz 1986). This evidence suggests that creatine is transported via some carrier-mediated transport process, rather than by passive diffusion, from the circulating blood to the retina against the concentration gradient between the retina and blood since creatine has a net positive charge and an estimated log partition coefficient of −2.7 (Persky and Brazeau 2001).

The characteristics of [^{14}C]creatine uptake by TR-iBRB2 cells support the belief that the creatine transport process is mediated by a secondary active transporter, since it is a Na^+-, Cl^-- and concentration-dependent process (Figs 3 and 4). The corresponding K_m value of 14.9 μM is in good agreement with an apparent K_m of 29 and 16 μM for rat and mouse CRT, respectively (Saltarelli *et al.* 1996; Ohtsuki *et al.* 2002). This K_m value is 10- to 40-fold lower than the plasma creatine concentration (140–600 μM) in the rat (Fitch and Shields 1966; Horn *et al.* 1998), suggesting that creatine transport is saturated by endogenous plasma creatine. This possibility further raises the question as to whether creatine is transported to the retina across the BRB. The intravenous administration of [^{14}C]creatine demonstrates that the $K_{p,app}(t)$ of the retina is greater than that of skeletal muscle and heart (Fig. 1b), which express CRT and undergo creatine uptake from the circulating blood (Murphy *et al.* 2001; Boehm *et al.* 2003). These results suggest that the creatine transport process at the BRB plays a key role in supplying creatine to the retina as CRT does in skeletal muscle and heart, even though CRT is completely saturated by plasma creatine. Although the blood-to-retina transport of [^{14}C]creatine in the presence of CRT specific inhibitors *in vivo* is direct evidence of creatine transport via CRT at the BRB, further inhibition cannot be predicted because of the plasma creatine concentration. Therefore, further studies are needed to investigate the blood-to-retina transport of [^{14}C]creatine using CRT knock-out mice.

The *in vitro* inhibition study suggests that CRT is involved in creatine transport, since β-guanidinopropionate and γ-guanidinobutyrate produce marked inhibition of [^{14}C]creatine uptake by TR-iBRB2 cells as reported elsewhere (Möller and Hamprecht 1989; Sora *et al.* 1994), but not of creatine metabolites, such as phosphocreatine and creatinine, and precursors, such as L-arginine (Table 1). RT-PCR and western blot analyses revealed that CRT mRNA and protein are expressed in rat retina and TR-iBRB2 cells as well as rat brain (Figs 5a and c). The bands at 85 kDa and 71 kDa seem to be glycosylated and non-glycosylated forms of CRT, respectively (Dodd and Christie 2001; Ohtsuki *et al.* 2002). Moreover, immunoperoxidase electron microscopic analysis revealed that CRT is localized at the luminal and abluminal membrane of rat retinal capillary endothelial cells (Fig. 6). The CRT immunoreactivity at the abluminal membrane tended to be greater than that at the luminal membrane. Similar evidence concerning GLUT1 determined by immunogold electron microscopy showed that GLUT1 expression at the abluminal membrane of rat retinal capillary endothelial cells is three-fold greater than that at the luminal membrane (Fernandes *et al.* 2003). It remains to be seen whether CRT at the abluminal membrane plays a role in transporting creatine in the blood-to-retinal direction and how RPE (outer BRB) contributes to the supply of creatine to the retina. Although further studies are needed to address these questions, our *in vivo* transport studies support the hypothesis that CRT at the luminal membrane transports creatine in the blood-to-retina direction (Fig. 1). Taking these results into consideration, CRT is localized in retinal capillary endothelial cells and plays an important role in transporting creatine from the circulating blood to the retina across the inner BRB. Our findings increase our understanding of the physiologic role of the BRB and the regulation of the creatine concentration in the retina in order to maintain ATP homeostasis in the neural retina which is required when there is a high metabolic demand.

Creatine deficiency syndromes, which involve an inborn deficiency of GAMT, AGAT, or creatine transporter 1 (SLC6A8, CT1, CRT1), cause depletion of creatine in the body (Schulze 2003). Except for an inborn deficiency of CRT1, our findings suggest that creatine is transported from the circulating blood to the retina in children with an inborn error of GAMT or AGAT by creatine replacement therapy. Oral administration of creatine is a potential treatment for neurodegenerative disease owing to the neuroprotective effects found in animal models of amyotrophic lateral sclerosis, Parkinson's disease, and Huntington's disease (Matthews *et al.* 1998, 1999; Klivenyi *et al.* 1999). These results suggest that CRT at the BBB plays an important role in supplying creatine to the brain (Ohtsuki *et al.* 2002). In contrast, in the long-term therapy of GA patients, the effect of creatine supplementation on the progression of eye symptoms appears to be small compared with the skeletal muscles (Vannas-Sulonen *et al.* 1985). The lack of agreement between GA patients and animal models for neurodiseases needs an explanation. Conceivably, creatine transport at the BRB is nearly saturated, even though the creatine plasma concentration is reduced in GA patients (Sipila *et al.* 1992). Another possibility is that CRT regulation at the BRB may occur during long-term therapy. This is because CRT expression at the plasma membrane and creatine uptake activity in the rat heart are reduced by creatine supplementation (Boehm *et al.* 2003). Moreover, translocation of CRT and creatine uptake activity appear to be affected by hormones, such as insulin-like growth factor I, insulin, and thyroid hormone (T_3) (Haugland and Chang 1975; Odoom *et al.* 1996; Steenge *et al.* 1998; Queiroz *et al.* 2002). Further studies are needed to elucidate the regulation of CRT expression and translocation at the plasma membrane of retinal capillary endothelial cells as far as efficient creatine supplementation therapy is concerned.

In conclusion, this study provides the first evidence that CRT, expressed in rat retinal capillary endothelial cells, is involved in the blood-to-retina influx transport of creatine. These findings regarding the creatine transport and CRT expression at the inner BRB are important for increasing our understanding of the mechanism governing the supply of creatine to the neural retina.

Acknowledgement

This study was supported, in part, by a Grant-in-Aid for Scientific Research from the Japan Society for the Promotion of Science.

References

Boehm E., Chan S., Monfared M., Wallimann T., Clarke K. and Neubauer S. (2003) Creatine transporter activity and content in the rat heart supplemented by and depleted of creatine. *Am. J. Physiol. Endocrinol. Metab* **284**, E399–E406.

Braissant O., Henry H., Loup M., Eilers B. and Bachmann C. (2001) Endogenous synthesis and transport of creatine in the rat brain: an in situ hybridization study. *Brain Res. Mol. Brain Res.* **86**, 193–201.

Cunha-Vaz J. G. (1976) The blood–retinal barriers. *Doc. Ophthalmol.* **41**, 287–327.

Defalco A. J. and Davies R. K. (1961) The synthesis of creatine by the brain of the intact rat. *J. Neurochem.* **7**, 308–312.

Dodd J. R. and Christie D. L. (2001) Cysteine 144 in the third transmembrane domain of the creatine transporter is located close to a substrate-binding site. *J. Biol. Chem.* **276**, 46983–46988.

Ennis S. R. and Betz A. L. (1986) Sucrose permeability of the blood–retinal and blood–brain barriers. Effects of diabetes, hypertonicity, and iodate. *Invest. Ophthalmol. Vis. Sci.* **27**, 1095–1102.

Fernandes R., Suzuki K. and Kumagai A. K. (2003) Inner blood–retinal barrier GLUT1 in long-term diabetic rats: an immunogold electron microscopic study. *Invest. Ophthalmol. Vis. Sci.* **44**, 3150–3154.

Fitch C. D. and Shields R. P. (1966) Creatine metabolism in skeletal muscle. I. Creatine movement across muscle membranes. *J. Biol. Chem.* **241**, 3611–3614.

Harris R. C., Soderlund K. and Hultman E. (1992) Elevation of creatine in resting and exercised muscle of normal subjects by creatine supplementation. *Clin. Sci. (Lond.)* **83**, 367–374.

Haugland R. B. and Chang D. T. (1975) Insulin effect on creatine transport in skeletal muscle (38464). *Proc. Soc. Exp. Biol. Med.* **148**, 1–4.

Horn M., Frantz S., Remkes H., Laser A., Urban B., Mettenleiter A., Schnackerz K. and Neubauer S. (1998) Effects of chronic dietary creatine feeding on cardiac energy metabolism and on creatine content in heart, skeletal muscle, brain, liver and kidney. *J. Mol. Cell. Cardiol.* **30**, 277–284.

Hosoya K., Kondo T., Tomi M., Takanaga H., Ohtsuki S. and Terasaki T. (2001a) MCT1-mediated transport of L-lactic acid at the inner blood–retinal barrier: a possible route for delivery of monocarboxylic acid drugs to the retina. *Pharm. Res.* **18**, 1669–1676.

Hosoya K., Tomi M., Ohtsuki S., Takanaga H., Ueda M., Yanai N., Obinata M. and Terasaki T. (2001b) Conditionally immortalized retinal capillary endothelial cell lines (TR-iBRB) expressing differentiated endothelial cell functions derived from a transgenic rat. *Exp. Eye Res.* **72**, 163–172.

Jones E. M. (1995) Na(+)- and Cl(−)-dependent neurotransmitter transporters in bovine retina: identification and localization by in situ hybridization histochemistry. *Vis. Neurosci.* **12**, 1135–1142.

Klivenyi P., Ferrante R. J., Matthews R. T., Bogdanov M. B., Klein A. M., Andreassen O. A., Mueller G., Wermer M., Kaddurah-Daouk R. and Beal M. F. (1999) Neuroprotective effects of creatine in a transgenic animal model of amyotrophic lateral sclerosis. *Nat. Med.* **5**, 347–350.

Mardashchev S. R. (1975) [Guanidinoacetate-*N*-methyltransferase: location in mammalian retina and rat Harderian gland]. *Biokhimiia* **40**, 353–357.

Marescau B., De Deyn P., Wiechert P., Van Gorp L. and Lowenthal A. (1986) Comparative study of guanidino compounds in serum and brain of mouse, rat, rabbit, and man. *J. Neurochem.* **46**, 717–720.

Matthews R. T., Yang L., Jenkins B. G., Ferrante R. J., Rosen B. R., Kaddurah-Daouk R. and Beal M. F. (1998) Neuroprotective effects of creatine and cyclocreatine in animal models of Huntington's disease. *J. Neurosci.* **18**, 156–163.

Matthews R. T., Ferrante R. J., Klivenyi P., Yang L., Klein A. M., Mueller G., Kaddurah-Daouk R. and Beal M. F. (1999) Creatine and cyclocreatine attenuate MPTP neurotoxicity. *Exp. Neurol.* **157**, 142–149.

Möller A. and Hamprecht B. (1989) Creatine transport in cultured cells of rat and mouse brain. *J. Neurochem.* **52**, 544–550.

Murphy R., McConell G., Cameron-Smith D., Watt K., Ackland L., Walzel B., Wallimann T. and Snow R. (2001) Creatine transporter protein content, localization, and gene expression in rat skeletal muscle. *Am. J. Physiol. Cell Physiol.* **280**, C415–C422.

Odoom J. E., Kemp G. J. and Radda G. K. (1996) The regulation of total creatine content in a myoblast cell line. *Mol. Cell. Biochem.* **158**, 179–188.

Ohtsuki S., Tachikawa M., Takanaga H., Shimizu H., Watanabe M., Hosoya K. and Terasaki T. (2002) The blood–brain barrier creatine transporter is a major pathway for supplying creatine to the brain. *J. Cereb. Blood Flow Metab.* **22**, 1327–1335.

Persky A. M. and Brazeau G. A. (2001) Clinical pharmacology of the dietary supplement creatine monohydrate. *Pharmacol. Rev.* **53**, 161–176.

Queiroz M. S., Shao Y., Berkich D. A., Lanoue K. F. and Ismail-Beigi F. (2002) Thyroid hormone regulation of cardiac bioenergetics: role of intracellular creatine. *Am. J. Physiol. Heart Circ. Physiol.* **283**, H2527–H2533.

Saltarelli M. D., Bauman A. L., Moore K. R., Bradley C. C. and Blakely R. D. (1996) Expression of the rat brain creatine transporter in situ and in transfected HeLa cells. *Dev. Neurosci.* **18**, 524–534.

Schulze A. (2003) Creatine deficiency syndromes. *Mol. Cell. Biochem.* **244**, 143–150.

Sipila I., Valle D. and Brusilow S. (1992) Low guanidinoacetic acid and creatine concentrations in gyrate atrophy of the choroids and retina (GA). In: *Guanidino Compounds in Biology and Medicine* (De Deyn, P. P., Marescau, B., Stalon, V. and Qureshi, I. A., eds), pp. 379–383. John Libbey Ltd, London.

Sora I., Richman J., Santoro G. *et al.* (1994) The cloning and expression of a human creatine transporter. *Biochem. Biophys. Res. Commun.* **204**, 419–427.

Steenge G. R., Lambourne J., Casey A., Macdonald I. A. and Greenhaff P. L. (1998) Stimulatory effect of insulin on creatine accumulation in human skeletal muscle. *Am. J. Physiol.* **275**, E974–E979.

Tomi M., Hosoya K., Takanaga H., Ohtsuki S. and Terasaki T. (2002) Induction of xCT gene expression and l-cystine transport activity by diethyl maleate at the inner blood–retinal barrier. *Invest. Ophthalmol. Vis. Sci.* **43**, 774–779.

Vannas-Sulonen K., Sipila I., Vannas A., Simell O. and Rapola J. (1985) Gyrate atrophy of the choroid and retina. A five-year follow-up of creatine supplementation. *Ophthalmology* **92**, 1719–1727.

Walker J. B. (1979) Creatine: biosynthesis, regulation, and function. *Adv. Enzymol. Relat. Areas Mol. Biol.* **50**, 177–242.

Wallimann T., Wegmann G., Moser H., Huber R. and Eppenberger H. M. (1986) High content of creatine kinase in chicken retina: compartmentalized localization of creatine kinase isoenzymes in photoreceptor cells. *Proc. Natl Acad. Sci. USA* **83**, 3816–3819.

Wyss M. and Kaddurah-Daouk R. (2000) Creatine and creatinine metabolism. *Physiol. Rev.* **80**, 1107–1213.

Yamaoka K., Tanigawara Y., Nakagawa T. and Uno T. (1981) A pharmacokinetic analysis program (multi) for microcomputer. *J. Pharmacobiodyn.* **4**, 879–885.

Yang W. X., Terasaki T., Shiroki K., Ohka S., Aoki J., Tanabe S., Nomura T., Terada E., Sugiyama Y. and Nomoto A. (1997) Efficient delivery of circulating poliovirus to the central nervous system independently of poliovirus receptor. *Virology* **229**, 421–428.

Molecular Vision 2004; 10:537-43 <http://www.molvis.org/molvis/v10/a66>
Received 16 April 2004 | Accepted 27 July 2004 | Published 9 August 2004

Retinal selectivity of gene expression in rat retinal versus brain capillary endothelial cell lines by differential display analysis

Masatoshi Tomi,[1,2] Hayato Abukawa,[1] Yoko Nagai,[3] Toshio Hata,[3] Hitomi Takanaga,[2,3,4] Sumio Ohtsuki,[2,3,4] Tetsuya Terasaki,[2,3,4] Ken-ichi Hosoya[1,2]

[1]Faculty of Pharmaceutical Sciences, Toyama Medical and Pharmaceutical University, Toyama, Japan; [2]Core Research for Evolutional Science and Technology (CREST) and Solution Oriented Research for Science and Technology (SORST) of the Japan Science and Technology Agency, Kawaguchi, Japan; [3]Department of Molecular Biopharmacy and Genetics, Graduate School of Pharmaceutical Sciences and the [4]New Industry Creation Hatchery Center, Tohoku University, Sendai, Japan

Purpose: The retina is a neural tissue especially differentiated for vision and, thus, the inner blood-retinal barrier (inner BRB) specific molecules may play an essential role in maintaining neural functions in the retina. The purpose of the present study was to identify selectively expressed genes at the inner blood-retinal barrier compared with the blood-brain barrier (BBB).

Methods: A comparison of expressed genes between conditionally immortalized rat retinal (TR-iBRB) cell lines and brain capillary endothelial (TR-BBB) cell lines was performed using mRNA differential display analysis and quantitative real time PCR analysis. The rat M-cadherin gene was cloned by performing 5' RACE, and its protein expression was detected by immunoblot analysis.

Results: Eight clones were identified as highly expressed genes in TR-iBRB cells including GATA-binding protein-3 (GATA-3), cytosolic branched chain amino transferase (BCATc), and M-cadherin (cadherin-15). The rat M-cadherin gene was cloned from TR-iBRB cells, for the first time, and has >86% amino acid sequence identity to the previously cloned mammalian M-cadherins. Rat M-cadherin expression in TR-iBRB cells was much greater than that in TR-BBB cells as far as mRNA and protein levels were concerned.

Conclusions: M-cadherin, GATA-3, and BCATc are highly expressed in TR-iBRB cells compared with TR-BBB cells and may indeed be involved in unique functions at the inner BRB.

In neural tissues like the retina and brain, the retinal and brain capillary endothelial cells form the inner blood-retinal (inner BRB) and blood-brain barriers (BBB), respectively. These barriers strictly regulate molecular transport between the circulating blood and neural tissues to maintain neural activities. It is believed that the molecules expressed at both barriers are almost identical and both barriers possess rigid tight-junctions to prevent the free diffusion of substances from the blood to neural tissues [1]. Several common transporters, such as D-glucose transporter 1 (GLUT1), creatine transporter (CRT), and P-glycoprotein, at both barriers are involved in the influx and efflux transport of essential substances and xenobiotics [2-7]. Nevertheless, the retina is especially differentiated for vision. This prompts the hypothesis that the inner BRB expresses different molecules from the BBB. We previously reported that the system x_c^- mediated L-cystine transport process is present at the inner BRB to protect the retina from light-induced oxidative stress, but it may not be at the BBB under normal conditions [8]. It is important to obtain more information about the inner BRB specific molecules, since they are intimately involved in retinal function.

Correspondence to: Ken-ichi Hosoya, Faculty of Pharmaceutical Sciences, Toyama Medical and Pharmaceutical University, 2630, Sugitani, Toyama, 930-0194, Japan; Phone: +81-76-434-7505; FAX: +81-76-434-5172; email: hosoyak@ms.toyama-mpu.ac.jp

We recently established conditionally immortalized rat retinal and brain capillary endothelial cell lines (TR-iBRB and TR-BBB cells, respectively) from transgenic rats harboring a temperature sensitive simian virus (SV) 40 large T-antigen gene [9,10]. TR-iBRB and TR-BBB cells possess endothelial markers and express GLUT1 and P-glycoprotein [9,10] which are expressed at the inner BRB and the BBB in vivo as shown by immunohistochemical analysis [2,3,6,7]. Thus, TR-iBRB and TR-BBB cells maintain certain in vivo functions and are a suitable in vitro model for the inner BRB and BBB, respectively [11].

The purpose of the present study was to identify selectively expressed genes at the inner BRB by mRNA differential display analysis of TR-iBRB and TR-BBB cells. The mRNA differential display technique works by systematic reverse transcription, polymerase chain reaction (PCR) amplification of the 3' termini of mRNAs, and resolution of those fragments on a polyacrylamide gel. This allows direct side-by-side comparison of the expressed genes under different conditions by using multiple primer combinations.

METHODS

Cell culture: TR-iBRB2, TR-iBRB9, TR-BBB11 and TR-BBB13 cells were established and characterized as described previously [9,10]. Cells were seeded onto rat tail collagen type I-coat tissue culture dishes (Becton Dickinson, Bedford, MA).

The cells were cultured in Dulbecco's modified Eagle's medium supplemented with 10% fetal bovine serum (Moregate, Bulimbra, Australia) and 15 µg/L endothelial cell growth factor (Roche Diagnostics, Mannheim, Germany) at 33 °C in a humidified atmosphere of 5% CO_2/air. The permissive-temperature for TR-iBRB and TR-BBB cell culture is 33 °C due to the presence of the temperature sensitive SV 40 large T-antigen in both cells.

mRNA differential display analysis: Differential display was performed using the rhodamine version of a fluorescence differential display kit (Catalog number 6626; Takara, Shiga, Japan). Briefly, total RNA was prepared from TR-iBRB2, TR-iBRB9, TR-BBB11 and TR-BBB13 cells using Trizol reagent (Invitrogen, Carlsbad, CA). DNase I was added to RNA in the presence of RNase inhibitor and incubated at 37 °C for 20 min to get rid of any potentially contaminating genomic DNA that would interefere with subsequent differential display. RNA (300 ng) was reverse transcribed with a rhodamine labeled arbitrary anchored oligo dT primer (5'-rhodamine labeled-T_nVV-3', where n=13-15, and V represents any base except T). The resulting cDNA was PCR amplified using 48 combinations of the rhodamine labeled arbitrary anchored oligo dT primer and an arbitrary decamer (5'-NNNNNNNNNN-3') through 35 cycles at 94 °C for 30 s, 40 °C for 2 min, and 72 °C for 1 min. PCR products were mixed with formamide loading buffer and incubated for 3 min at 94 °C prior to loading on to 6% polyacrylamide gels. Gels were run at 30 W constant current, and DNA bands were visualized using a fluorescent image analyzer (FLA3000; Fujifilm, Tokyo, Japan). DNA bands differentially displayed between TR-iBRB and TR-BBB cells were excised from the gel and boiled in water for 30 min. The eluted DNA was reamplified using the same primer set and PCR conditions. Reamplified PCR products were run on 3% agarose gel containing H. A.-Yellow™ (Catalog number HA002, Takara) and visualized using the fluorescent image analyzer. H. A.-Yellow selectively binds to AT base pairs, and thus loaded DNA fragments are separated according to their AT contents. Differentially displayed DNA bands were excised and the DNA was eluted using spin columns (Ultrafree-DA; Millipore, Billerica, MA). The eluted DNA was cloned into a plasmid (pBluescript SKII+; Stratagene, La Jolla, CA), and amplified in *E. coli*. Several clones were sequenced in both directions using a DNA sequencer (model 4200; Li-COR, Lincoln, NE). Similarities with other sequences in GenBank were examined using the BLAST program at the National Center for Biotechnology Information.

Quantitative real time PCR analysis: Quantitative real time PCR for specific genes was performed to confirm the differences in genes identified by differential display analysis. Single-strand cDNA was synthesized from TR-iBRB2, TR-iBRB9, TR-BBB11 and TR-BBB13 cell total RNA (1 µg) by reverse transcription using oligo dT as the primer. According to the manufacturer's protocol, quantitative real time PCR was performed using an ABI PRISM 7700 sequence detector system (PE-Applied Biosystems, Foster City, CA) with a 2X SYBR Green PCR master mix (PE-Applied Biosystems), reverse transcribed cDNA, and gene specific primers. To quantify the amount of target mRNA in the samples, a standard curve was prepared for each run using the plasmid containing the target gene. This enabled standardization of the initial mRNA content of cells relative to the amount of glyceraldehyde-3-phosphate dehydrogenase (GAPDH). The sequences of the specific primers were as follows: the sense sequence was 5'-GTT CAC CAA GGA TGA GTT CTT TAT GG-3' and the antisense sequence was 5'-AGG ATG GTG AAC CTG GCC ACC CAG TT-3' for rat M-cadherin, and the sense sequence was 5'-TGA TGA CAT CAA GAA GGT GGT GAA G-3' and the antisense sequence was 5'-TCC TTG GAG GCC ATG TAG GCC AT-3' for GAPDH. The data represent means±standard error of the mean. Statistical significance of differences among means of several groups was determined by one way analysis of variance (ANOVA) followed by the modified Fisher's least squares difference method.

5' Rapid amplification of cDNA ends (5' RACE): Since differential display could only identify the 3' terminal of mRNAs, the 5' sequence was amplified using total RNA of TR-iBRB2 cells, a SMART RACE cDNA amplification kit (CLONTECH, Palo Alto, CA), and the clone 1 (Table 1) specific reverse primer (5'-AGA TGC CTG CTT TCA TAC AGA GGT GA-3'), according to the manufacturer's protocol. The

Table 1. Genes highly expressed in TR-iBRB cells

Clone number	Expression ratio	Clone length	Sequence type	Accession number	Species	Name	Gene locus (Rat)
1	213	251 bp	mRNA	NM_007662	Mouse	M-cadherin (Cadherin-15)	19q12
2	23.9	437 bp	mRNA	NM_008091	Mouse	GATA-binding protein 3 (GATA-3)	17q12.3
3	20.0	358 bp	Genome	NW_047695	Rat		4q34
4	5.46	114 bp	mRNA	AJ278701	Rat	Cytosolic branched chain amino transferase (BCATc)	4q44
5	4.54	355 bp	Genome	NW_047430	Rat		14q22
6	4.00	209 bp	EST	Rn.954 (UniGene)	Rat	Transcribed sequences	15p11
7	3.25	193 bp	Genome	NW_048042	Rat		Xq22
8	2.44	102 bp	Genome	NW_047657	Rat		3q34

Selectively expressed genes in TR-iBRB cells were identified by mRNA differential display and quantitative real time PCR analyses. Expression ratio represents ratio of mRNA level between TR-iBRB and TR-BBB cells (TR-iBRB/TR-BBB).

purified 5' RACE PCR product was cloned into a plasmid (pBluescript SKII+) and then amplified in *E. coli*. Several clones were sequenced from both directions using a DNA sequencer.

Immunoblot analysis: Protein samples were obtained by dissolving cells in lysis buffer consisting of 1% sodium dodecyl sulfate (SDS), 10 mM Tris-HCl (pH 6.8), 10% glycerol, 1 mM EDTA, and 10 µL/mL protease inhibitor cocktail (Sigma, St. Louis, MO). Protein samples were boiled for 10 min and centrifuged at 8,000x g for 10 min at 4 °C. Supernatants were separated and used as a whole cell extract. The proteins (100 µg) were electrophoresed on an SDS-polyacrylamide gel and subsequently electrotransferred to a poly vinylidene difluoride membrane. The membranes were incubated with goat polyclonal anti-human M-cadherin antibody (1:500; Santa Cruz Biotechnology, Santa Cruz, CA) for 16 h at 4 °C as the primary antibody using blocking agent solution (Block Ace; Dainihon Pharmaceutical Co., Osaka, Japan). There was apparently sufficient antibody cross-reactivity between human and rat M-cadherin. The membranes were subsequently incubated with horseradish peroxidase conjugated anti-goat IgG as the secondary antibody. The bands were visualized with an enhanced chemiluminescence kit (Amersham, Buckinghamshire, UK).

RESULTS

The differential display analysis of TR-iBRB2, TR-iBRB9, TR-BBB11, and TR-BBB13 cells showed 40 bands, which were selectively expressed more in TR-iBRB cells than in the TR-iBBB cells (Figure 1A). These DNA bands of 100 to about 450 bp were cloned and sequenced. Quantitative real time PCR using specific primers for each clone was performed to confirm the reproducibility. As a result of these analyses, eight clones were identified and found to be expressed to a greater extent in TR-iBRB cells than in TR-BBB cells (Table 1). The differential displayed clones included two sequences homologous to mouse genes, such as M-cadherin (cadherin-15; clone 1), GATA-binding protein 3 (GATA-3; clone 2), and one sequence identical to rat cytosolic branched chain amino transferase (BCATc; clone 4). The other five sequences (clones 3, 5, 6, 7, and 8) were only found in the expressed sequence tag (EST) or genomic sequences.

Clone 1, of 251 bp, which was expressed 213 fold more intensely in TR-iBRB cells than in TR-BBB cells, exhibited

B:

```
Clone 1             1 TTTTTGGCTCCATGGCAGATAAACTCACTGAAGGTCATCTGTGTGAGCTCC   51
Mouse M-cadherin 3080 --------------------------------------------------- 3080

Clone 1            52 AGGGGAGGACTGAGTCCTGTATGGGCTAGGCAGCG-GAGGGAGAGCGCTCT  101
Mouse M-cadherin 3080 -------------------ATGGACTAGGCAGCTAGAGGGAGCACTGTCC 3110
                                          **** *********  ******* *  **

Clone 1            102 CCCTCTGGAGTGCAGAAGCCACC-TTCAATCACCCTGCTAGGGTTCATCCC  151
Mouse M-cadherin 3111 TGGCA--GAGTGCAGAAGCCACCCTTAGTG--CCCTGCTAGGGCTCATCCC 3157
                      ***************** **      *********** *******

Clone 1            152 ATCTTTGTGTCCCAGTTGTGACTCTCACCTCTGTATGAAA-GCAGGCATCT  201
Mouse M-cadherin 3158 ATCTTTGATTCCCAGTTGTGACTCTTGCCTCTGTATGAAAAGCAGGCGTCT 3208
                      *******  ***************  ************* ****** ***

Clone 1            202 AAGGAGCAGATTGGAATTAAAAACA-ACTGTTCAGTGAAAAAAAAAAAAAA  251
Mouse M-cadherin 3209 AAAGAGTGGATTTCAATTAAAAGCATACTATTTGGGGGATCCAAAAAAAA  3258
                      ** ***  ****  ******** ** *** **  * * *  ********
```

Figure 1. Differential display analysis of TR-iBRB and TR-BBB cells. A: Typical fluorescent image of polyacrylamide gel electrophoresis. An arrow indicates selectively expressed DNA bands in TR-iBRB cells. DNA bands were cloned and sequenced. B: Nucleotide sequence of the selectively expressed clone (clone 1) marked by the arrow in A. Clone 1 sequence after nucleotide position 72 has 77% nucleotide homology with the 3' terminal of the mouse M-cadherin gene.

the largest difference in mRNA expression level of the eight clones. The sequence of clone 1 following nucleotide position 72 exhibited 77% nucleotide identity to the 3' terminal of the mouse M-cadherin gene (Figure 1B) [12]. By performing 5' RACE, a 2686 bp cDNA fragment was amplified as a rat M-cadherin. This sequence includes the clone 1 sequence and an open reading frame of 2355 nucleotides, which corresponds to 784 amino acid residues (Figure 2). The deduced amino acid sequence exhibits 97% and 86% identity to mouse and human M-cadherin, respectively [12,13], suggesting that the amplified DNA fragment represents the rat homolog of the M-cadherin gene.

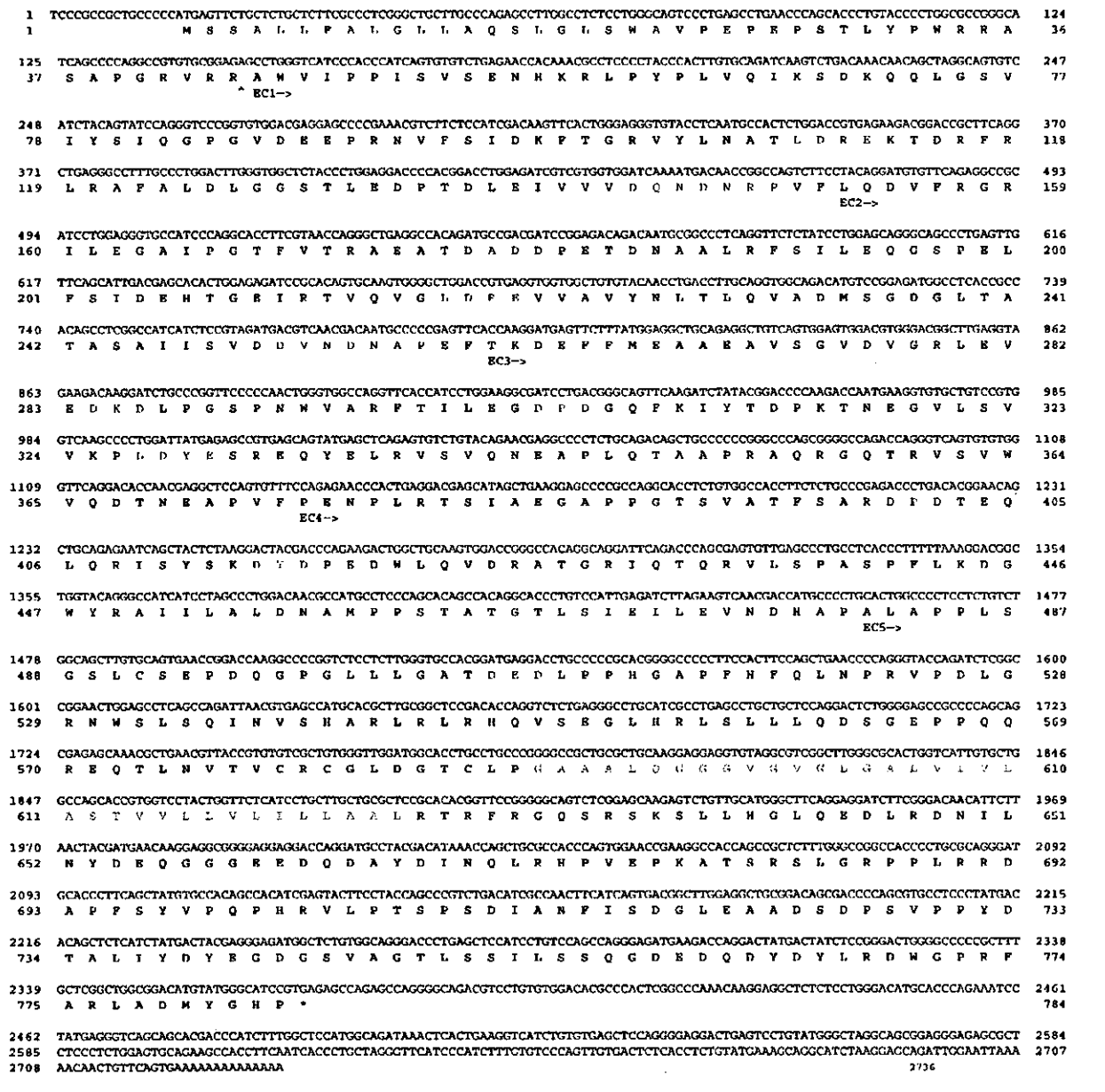

Figure 2. Nucleotide and deduced amino acid sequences of rat M-cadherin. The deduced amino acid sequence is shown below the nucleotide sequence. The stop codon is denoted by an asterisk. The signal peptide is in blue and the postulated furin cleavage site of the precursor polypeptides is indicated by a ^. The extracellular domain is divided into five cadherin extracellular subdomain repeats (*EC1-EC5*). The transmembrane domain is in green. In the cytoplasmic domain following the transmembrane domain, the membrane-proximal conserved domain (MPCD) is in purple and the catenin binding sequence (CBS) is in orange. The characteristic cadherin consensus sequences are shaded in red. The 4 cysteine residues in EC5 are in pink. The *N*-glycosylation sites are indicated in brown. The nucleotide sequence of rat M-cadherin is in GenBank with the accession number AB176538.